

**SILICA IMMOBILIZED PORPHYRIN-CuInS₂/ZnS QUANTUM DOT CONJUGATES
FOR COLIFORM BACTERIA PHOTOINACTIVATION IN WATER**

by

KNOWLEDGE SIYABONGA NDLOVU

Submitted in accordance with the requirements for the degree of

MASTER OF SCIENCE

in

CHEMISTRY

at the

UNIVERSITY OF SOUTH AFRICA

SUPERVISOR: DR. MUTHUMUNI E. MANAGA

CO-SUPERVISORS: PROF. MAKWENA J. MOLOTO

DR. KUTLOANO E. SEKHOSANA

DATE OF SUBMISSION: 26 JANUARY 2024

DECLARATION

Name: KNOWLEDGE SIYABONGA NDLOVU
Student number: 14797585
Degree: Master of Science: Chemistry

Exact wording of the title of the dissertation or thesis as appearing on the copies submitted for examination:

**SILICA IMMOBILIZED PORPHYRIN-CuInS₂/ZnS QUANTUM DOT CONJUGATES
FOR COLIFORM BACTERIA PHOTOINACTIVATION IN WATER**

I declare that the above dissertation is my own work and that all the sources that I have used or quoted have been indicated and acknowledged by means of complete references.

I further declare that I submitted the dissertation to originality checking software and that it falls within the accepted requirements for originality.

I further declare that I have not previously submitted this work, or part of it, for examination at Unisa for another qualification or at any other higher education institution.



SIGNATURE

26/01/2024

DATE

DEDICATION

I would like to dedicate this dissertation to the following:

1. The science community of Africa and the world at large.
2. My family that guides, supports and teaches me spiritual lessons.

“IT ALWAYS SEEMS IMPOSSIBLE UNTIL IT’S DONE.” - Nelson Mandela

PUBLICATIONS

PUBLICATIONS:

- Ndlovu, KS, Moloto, MJ, Sekhosana, KE, Nkambule, TTI and Managa, M. 2023. Porphyrins developed for photoinactivation of microbes in wastewater. *Environmental Science and Pollution Research*. 30: 11210-11225.
- Ndlovu, KS, Chokoe K, Masebe T, Sekhosana KE, Moloto MJ, Managa M. 2023. Photoinactivation of Escherichia coli and Staphylococcus aureus using Porphyrin-CuInS₂/ZnS quantum dot conjugates immobilized on Mesoporous Silica. *Accepted for publication*. Chemical Papers (Manuscript number: CHPA-D-23-03677).

CO-AUTHORSHIPS:

- Ledwaba, MM, Magaela, NB, Ndlovu, KS, Mack, J, Nyokong, T & Managa, M. 2022. Photophysical and in vitro photoinactivation of Escherichia coli using cationic 5,10,15,20-tetra(pyridin-3-yl) porphyrin and Zn(II) derivative conjugated to graphene quantum dots. *Photodiagnosis and Photodynamic Therapy*. 40:103127.
- Magaela, BN, Ndlovu, KS, Tshangana, CS, Muleja, AA, Mamba, BB, Nyokong, T & Managa, M. 2022. Photodegradation of ibuprofen using 5-10-15-20-tetrakis(4-bromophenyl) porphyrin conjugated to graphene quantum dots. *Optical Materials*. 134(PA):113147.

ACKNOWLEDGEMENTS

The following people and organizations deserve my deepest gratitude for assisting in making this study a success:

- I would like to recognize the project supervisors starting with Dr Muthumuni Managa, for rousing me with her commitment, for driving by case and for setting a tall standard to take after. I would like to thank her for being persistent with me and pushing me past my claim limits. I would moreover like to expand my appreciation to Prof Makwena Moloto for academic support and liaising with other departments for instrument access. Lastly, I would like to thank Dr Kutloano Sekhosana for his academic support, guidance and development .I appreciate the team's commitments to the project, and the penances they made in making beyond any doubt that it is a success.
- I would like to acknowledge the iNanoWS laboratory technical team for the role they played in making this work a success. Ms Nontokozo Magwaza, Mr Siyabonga Mhlongo and Mr Zamani Ncanana for always being available to assist me and making sure that I can conduct my experiments effectively. Your dedication has made it possible for all the students to work effectively and productively in the labs and for that we are grateful.
- I would also like to appreciate iNanoWS staff and students that have contributed to the success of this project. Thanks to Ms Gcinaphi Shabalala and Mr Halahala Mbongo for assisting us with the administrative tasks throughout our studies.
- I would like to thank everyone in my family and friends for supporting me financially, spiritually and praying for my success and accompanying me on this journey.
- I would like to express my deep gratitude to the University of South Africa, the Institute for Nanotechnology and Water Sustainability and the Department of Life and Consumer Sciences, College of Agriculture and Environmental Sciences (CAES) for giving me the opportunity to learn and develop and for funding the project.

- The Council for Scientific and Industrial Research (CSIR) is also acknowledged for grant funding through their Laser Rental Pool Program (RPP). Grant holder: Dr ME Managa.
- The Women in Research (WIR) support program from UNISA is also appreciated for funding that assisted this project for external analysis.



ABSTRACT

Chlorination is a widely used chemical disinfection technique in South African water treatment facilities. However, it fails to combat emerging pollutants, drug resistant microbes and carcinogenic by-products, resulting in the inability of water treatment plants (WTPs) to meet standard regulations. Thus, alternative techniques to combat these challenges must be developed. Among the reported procedures, antimicrobial photodynamic inactivation (aPDI) is reportedly promising. aPDI is a photoinactivation technique employed for combating prevalent and drug-resistant pathogenic microbes. The efficacy of aPDI is independent of existing drug-resistance and is not associated with promoting drug-resistance after a photoinactivation process. In this study, the synthesis, characterization, photochemical properties and aPDI efficacy of a metal-free and indium (III) porphyrin conjugated to CuInS₂/ZnS core-shell quantum dots (QDs) against *E. coli* and *S. aureus* when immobilized on mesoporous silica is reported. The effect of conjugation and metalation of porphyrin with indium (III) on aPDI efficacy, singlet oxygen quantum yields, fluorescence lifetimes, fluorescence quantum yields, triplet lifetimes and antimicrobial log reductions was studied.

This study finds indium (III) porphyrin and CuInS₂/ZnS QDs to generate more reactive oxygen species and singlet oxygen through conjugation. The singlet oxygen quantum yield of nanoconjugates was determined to be higher when compared to non-conjugated porphyrins. As such, the photoinactivation efficacy of nanoconjugates was greater.

SILICA IMMOBILIZED PORPHYRIN-CuInS₂/ZnS QUANTUM DOT CONJUGATES FOR COLIFORM BACTERIA PHOTOINACTIVATION IN WATER

KEY TERMS: *Escherichia coli*; *Staphylococcus aureus*; Porphyrin; Quantum dots; Antimicrobial photodynamic inactivation; Mesoporous silica; Photoinactivation; Nanoconjugate; Immobilization; Coliform bacteria; Wastewater

TABLE OF CONTENTS

DECLARATION.....	2
DEDICATION.....	3
PUBLICATIONS.....	4
ACKNOWLEDGEMENTS.....	5
ABSTRACT.....	7
TABLE OF CONTENTS.....	9
LIST OF ABBREVIATIONS.....	12
LIST OF SYMBOLS.....	14
CHAPTER 1.....	15
INTRODUCTION.....	15
1.1 BACKGROUND.....	15
1.2 PROBLEM STATEMENT.....	16
1.3 JUSTIFICATION.....	17
1.4 AIMS AND OBJECTIVES.....	18
1.5 DISSERTATION OUTLINE.....	19
1.6 REFERENCES.....	19
CHAPTER 2.....	22
LITERATURE REVIEW.....	22
2.1 INTRODUCTION.....	22
2.1.1 THE WATER TREATMENT PROCESS.....	22
2.1.2 MICROBES IN WATER TREATMENT.....	23
2.1.3 TYPES OF BACTERIA.....	24
2.2 QUANTUM DOTS.....	25
2.3 PORPHYRINS.....	27
2.3.1 SYNTHETIC ROUTES OF PORPHYRINS.....	28
2.3.2 METALATION.....	29
2.3.3 PHOTSENSITIZATION.....	30
2.3.4 PHOTOINACTIVATION ACTIVITY.....	32
2.4 REFERENCES.....	34
CHAPTER 3.....	37
EXPERIMENTAL METHODOLOGY.....	37
3.1 INTRODUCTION.....	37
3.2 MATERIALS, REAGENTS AND SOLVENTS.....	37
3.3 INSTRUMENTATION.....	37

3.4	PHOTOSENSITIZER (PORPHYRIN) SYNTHESIS.....	40
3.5	NANOPARTICLE SYNTHESIS.....	42
3.5.1	SYNTHESIS OF CuInS ₂ /ZnS CORE/SHELL QUANTUM DOTS FUNCTIONALIZED WITH GLUTATHIONE.....	42
3.5.1.1	FIRST ATTEMPT.....	42
3.5.1.2	SECOND ATTEMPT.....	43
3.8	SAMPLING AND PREPARATION.....	45
3.9	DNA EXTRACTION, QUATIFICATION AND PCR AMPLIFICATION.....	47
3.10	PHOTOINACTIVATION.....	48
3.10.1	NANOCONJUGATE.....	48
3.10.2	LIGHT SIMULATION.....	49
3.11	REFERENCES.....	49
CHAPTER 4.....		51
RESULTS AND DISCUSSIONS: CHARACTERIZATION AND PHOTO- PHYSICOCHEMICAL STUDIES.....		51
4.1	INTRODUCTION.....	51
4.2	CHARACTERIZATION.....	51
4.2.1	Nuclear magnetic resonance (NMR), mass spectrometry (MS) and Fourier- transform infrared (FTIR) spectroscopy.....	51
4.2.2	UV/Vis spectroscopy.....	54
4.2.3	Fluorescence emission spectra.....	59
4.2.4	Dynamic light scattering (DLS).....	60
4.2.5	X-ray diffraction (XRD).....	61
4.2.5	Thermogravimetric analysis (TGA).....	63
4.2.6	N ₂ sorption studies.....	64
4.2.7	Scanning electron microscopy (SEM).....	65
4.2.7	Energy dispersive microscopy (EDS).....	67
4.2.8	Fluorescence lifetimes (τ_F) and quantum yield (Φ_F).....	68
4.2.9	Singlet oxygen quantum yield (Φ_Δ).....	70
4.2.10	Triplet lifetime (τ_T).....	71
4.3	REFERENCES.....	72
CHAPTER 5.....		74
ANTIMICROBIAL STUDIES.....		74
5.1	INTRODUCTION.....	74
5.2	METAGENOMIC DATA.....	74
5.3	<i>IN VITRO</i> ANTIMICROBIAL STUDIES.....	78

5.3 REFERENCES	82
CHAPTER 6.....	83
CONCLUSIONS AND RECOMMENDATIONS	83
6.1 CONCLUSIONS	83
6.2 RECOMMENDATIONS	84

LIST OF ABBREVIATIONS

¹H-NMR	Proton Nuclear Magnetic Resonance
ADMA	Anthracene-9,10-diyl-bis-methylmalonate
CFU	Colony forming units
CIS	Copper indium sulfide
DBPs	Disinfection by-products
DCC	N,N-dicyclohexylcarbodiimide
DCM	Dichloromethane
DLS	Dynamic light scattering
DMA	9,10-dimethylantracene
DMF	Dimethylformamide
DMSO	Dimethylsulfoxide
DMSO-d₆	Deuterated dimethylsulfoxide
DNA	Deoxyribonucleic acid
<i>E. coli</i>	<i>Escherichia coli</i>
<i>E. faecalis</i>	<i>Enterococcus faecalis</i>
EDS	Energy dispersive X-ray spectroscopy
FDA	Food and Drug Administration
FTIR	Fourier-transform infrared spectroscopy
ISC	Intersystem crossing
LED	Light-emitting diode
NPs	Nanoparticles
OLA	Oleic acid
OLM	Oleyamine
<i>P. aeruginosa</i>	<i>Pseudomonas aeruginosa</i>
PCR	Polymerase chain reaction
PS	Photosensitizer
PSs	Photosensitizers
RB	Rose Bengal

RNA	Ribonucleic acid
ROS	Reactive oxygen species
<i>S. aureus</i>	<i>Staphylococcus aureus</i>
TCSPC	Time Correlated Single Proton
TGA	Thermogravimetric analysis
THMs	Trihalomethanes
UV-Vis	Ultraviolet-visible spectroscopy
XRD	X-ray powder diffraction
ZnTPP	Zinc tetraphenylporphyrin

LIST OF SYMBOLS

*S	Singlet excited state
¹O₂	Singlet excited oxygen
³O₂	Molecular oxygen
Abs	Absorbance/absorption
e⁻	Electron
H⁺	Proton
φ_Δ	Singlet oxygen quantum yield
φ_F	Fluorescence quantum yield
S₀	Singlet ground state
t	Time
T₃	Triplet excited state
α	Non-peripheral position
β	Peripheral position
ε	Molar extinction coefficient
ζ	Zeta potential
λ	Wavelength
τ_F	Fluorescence lifetime

CHAPTER 1

INTRODUCTION

1.1 BACKGROUND

The Water Research Commission (WRC) is dedicated to delivering reliable and cost-effective innovations to enhance wastewater management, ultimately contributing to improvements in social, economic, and health sectors. Its objectives are centred around the development of technologies aimed at enhancing the quality of water supplied to households and industries alike. Improving wastewater treatment processes for increased reusability and quality is therefore a top priority (Carlsson, 2003).

Currently, Wastewater Treatment Plants (WWTPs) commonly use chlorination as a preferred disinfection method, especially in South Africa (Carlsson, 2003). Chlorination is effective in achieving regulatory standards for domestic and industrial consumption, but the long-term effects are not desirable (Nieuwenhuijsen et al., 2009a). Chlorination forms trace concentrations of trihalomethanes proven carcinogenic to human beings and poses a health risk (Evlampidou et al., 2020). Moreover, conventional wastewater treatment processes are not qualified in eradicating contaminants of emerging concern (CECs) such as pharmaceuticals, algal toxins, antibiotic resistant bacteria and pesticides (Pastorino and Ginebreda, 2021). CECs not only endanger human health but also pose significant risks to the environment (Yadav et al., 2021). Current wastewater treatment plants (WWTP) often lack major technological solutions to mitigate or eliminate these risks associated with longtime chlorination use in wastewater treatment (Necibi et al., 2021). Hence, it is essential to conduct research aimed at identifying and implementing cost-effective alternatives to support or replace chlorination methods.

Bacteria is an abundant pathogenic microbe in WWTP influent. Therefore, it is important to focus on bacteria when studying new disinfection technologies for addressing concerns related to chlorination (Makuwa et al., 2023). Recent technologies involve the usage of photosensitizers (PSs) and nanoparticles (NPs) for aPDI (Alves et al., 2015). The technique uses light absorption for photocatalytic production of reactive oxygen species (ROS) to inactivate bacteria (Manoharan et al., 2022). Porphyrins (photosensitizer) and QDs (nanoparticle) have demonstrated

desirable antibacterial characteristics such as long fluorescence lifetimes, large Stokes shift, efficient ROS generation and a broad range of emission, making them suitable candidates for next-generation antibacterial agents (B. N. Magaela et al., 2022; Sen et al., 2022). Furthermore, porphyrins and QDs can be functionalized and conjugated to enhance their antibacterial efficacy, reduce toxicity and limit leaching (Ndlovu et al., 2022). This study aims at conjugating porphyrins to QDs and using mesoporous silica for immobilization to prevent negative environmental impacts.

1.2 PROBLEM STATEMENT

Many WWTPs are considered competent in delivering satisfactory water standards for domestic and industrial use. This is assessed through qualitative and quantitative analysis of coliform bacteria and other related pollutants after a treatment process. Coliform bacteria are monitored because it acts as an indicator for the presence of other microbes (Luyt et al., 2012). WWTPs then employ disinfection methods to reduce the levels of microbes to a safe minimum prescribed levels. Chemical disinfection through chlorination is the commonly used method. Meanwhile studies show various microbes to be resistant towards chlorination (Jin et al., 2020). This occurs at low chlorine concentrations and through spontaneous mutations that aid resistance development. In addition, disinfection by-products (DBPs) are a growing concern related to chlorination (Nieuwenhuijsen et al., 2009b). Chlorine will react with natural organic matter to form carcinogenic trihalomethanes (THMs) such as chloroform, bromoform, bromodichloromethane and dibromochloromethane if the environment allows (Clayton et al., 2019). These new findings question the efficiency of chlorination and thus seek supplementation.

Research has shown that QDs can successfully inactivate bacteria via ROS generation. CdSe and PbTe QDs form part of traditional binary QDs previously used in antibacterial studies (Tsolekile et al., 2017). Binary QDs comprise of group II-VI and IV-VI elements, which are now considered toxic due to the presence of heavy metals. Ternary QDs have become a safer alternative as they comprise of group I-II-VI elements (e.g., CuInS₂) (Tsolekile et al., 2017). These QDs have a higher limit of toxicity risk at 4200 mg/kg. Therefore, they are better candidates for disinfection and environmental applications. Other disinfection materials with outstanding efficacy

involves organic photosensitizers (PSs). Challenges encountered when using QDs and PSs include photobleaching and complex recovery mechanisms such as adsorption, filtration and photocatalysis (Thandu et al., 2015). Photobleaching occurs when molecules lose their fluorescence due to prolonged exposure to light. This can be tackled by using photostable PSs like porphyrins due to a unique chemical structure that enhances stability and prevents light-induced degradation. On the other hand, mesoporous silica is good for the recovery and reuse aspect because of its porosity, high surface area, stability and renderability.

1.3 JUSTIFICATION

Water and sanitation departments of South African municipalities fail to meet microbial compliance for both drinking water and sewage as of 11 October 2022 on the Department of Water and Sanitation regulatory dashboard. Pathogenic bacteria are still the main cause of water pollution, with their presence rendering water of poor quality and unsuitable for human use, potentially leading to water-borne diseases (Mudau et al., 2023). This is compounded by chlorination, a widely used and globally recognized treatment method, leading to antibiotic resistance (Jin et al., 2020). Moreover, the regulated quantity of trihalomethanes (THMs) is higher in South Africa when compared to regulations of European countries for example. Even with lower limits, European countries report cancer-related health cases promoted by THMs through chlorination of drinking water. As South African WTPs fail to meet various regulations, there's a higher risk of adverse effects on human health and the environment.

Antimicrobial photodynamic inactivation (aPDI) is an innovative method that utilizes oxidative stress to inactivate various microbes (Pucelik and Dąbrowski, 2022). This technique holds advantages of preventing microbial resistance, low toxicity, cost-effective and does not promote DBPs (Hamblin, 2016). Therefore, aPDI can be employed to investigate its efficacy on microbial photoinactivation and addressing concerns related to chlorination. Nanoparticles such as titanium dioxide and porphyrins are commonly used in water treatment processes. Through photocatalysis, degradation of pollutants is achieved when light is induced. Innovative quantum dot-porphyrin conjugate materials have great potential to solve the limitations of current

disinfection methods. Thus far, no reported study has been conducted that combines the photoinactivation capabilities of porphyrins and QDs whilst immobilized on mesoporous silica for recovery and reuse.

1.4 AIMS AND OBJECTIVES

This study was aimed at synthesizing and conjugating QDs with porphyrins to achieve significant bacterial inactivation by phototreatment of wastewater through combining their desirable properties.

The following specific objectives were followed to achieve the aims:

- Synthesis and characterization of metal-free and Indium (III) derivative of 4-(15-(4-boronophenyl)-10,20-diphenylporphyrin-5-yl)benzoic acid, CuInS₂/ZnS quantum dots and mesoporous silica.
- Synthesis and characterization of silica immobilized CuInS₂/ZnS quantum dots conjugated metal-free and Indium (III) derivative of 4-(15-(4-boronophenyl)-10,20-diphenylporphyrin-5-yl)benzoic acid.
- Phototreatment of *Escherichia coli* and *Staphylococcus aureus* with the synthesized nanoconjugate
- Examination of the photo-physicochemical properties and antibacterial activity of the nanoconjugate

1.5 DISSERTATION OUTLINE

CHAPTER 1	Introduction: This chapter is focused on the preface of the study. The background, aims and objectives, problem statement, justification and dissertation outline are stated in this chapter.
CHAPTER 2	Literature review: An overview of the water treatment process utilized in South Africa and worldwide is outlined in this chapter. It evaluates the advantages and disadvantages of current disinfection methods on human health, the environment and effectuality. Conventional disinfection methods are discussed, and their pros and cons evaluated as well. Lastly, attempts of improving the short-falls of conventional disinfection methods are explored.
CHAPTER 3	Experimental methodology: The experimental procedures followed to attain the objectives of this study are dispensed in this chapter. Materials, methods of synthesis, instrumentations, successful and unsuccessful attempts are discussed in this chapter.
CHAPTER 4	Results and discussions: Results from various characterization techniques and photophysiochemical studies are provided. This is based on the successful experimental methodology that was followed.
CHAPTER 5	Antibacterial studies: Photoinactivation of <i>escherichia coli</i> and <i>staphylococcus aureus</i> using the synthesized conjugates is discussed in this chapter. Further discussions include the performance and efficacy of the conjugates as a disinfection method.
CHAPTER 6	Conclusions and recommendations: This chapter provides the concluding remarks, findings of the study and further research recommendations focused on this field.

Figure 1.1. Dissertation outline.

1.6 REFERENCES

Alves, E., Faustino, M.A.F., Neves, M.G.P.M.S., Cunha, Â., Nadais, H., Almeida, A., 2015. J. Photochem. Photobiol. C Photochem. Rev. 22, 34–57.

Carlsson, F.H.H., 2003. Elementary handbook of water disinfection.1, 11-14.

Clayton, G.E., Thorn, R.M.S., Reynolds, D.M., 2019. Front. Environ. Sci. 7. 1362-1378.

Evlampidou, I., Font-Ribera, L., Rojas-Rueda, D., Gracia-Lavedan, E., Costet, N., Pearce, N., Vineis, P., Jaakkola, J.J.K., Delloye, F., Makris, K.C., Stephanou, E.G., Kargaki, S., Kozisek, F., Sigsgaard, T., Hansen, B., Schullehner, J., Nahkur, R., Galey, C., Zwiener, C., Vargha, M., Righi, E., Aggazzotti, G., Kalnina, G., Grazuleviciene, R., Polanska, K., Gubkova, D., Bitenc, K., Goslan, E.H., Kogevinas, M., Villanueva, C.M., 2020. *Environ. Health Perspect.* 128. 2096-2132.

Hamblin, M.R., 2016. *Curr. Opin. Microbiol.* 33, 67–73.

Jin, M., Liu, L., Wang, D., Yang, D., Liu, W., Yin, J., Yang, Z., Wang, H., Qiu, Z., Shen, Z., Shi, D., Li, H., Guo, J., Li, J., 2020. *ISME Journal.* 14, 1847–1856.

Luyt, C.D., Tandlich, R., Muller, W.J., Wilhelmi, B.S., 2012. *Int. J. Environ. Res. Public Health* 9, 2669–2693.

Magaela, B.N., Ndlovu, K.S., Tshangana, C.S., Muleja, A.A., Mamba, B.B., Nyokong, T., Managa, M., 2022. *Opt. Mater. (Amst).* 134, 113147.

Makuwa, S., Green, E., Fosso-Kankeu, E., Moroaswi, V., Tlou, M., 2023. *Appl. Microbiol.* 3, 764–773.

Manoharan, R.K., Raorane, C.J., Ishaque, F., Ahn, Y.-H., 2022. *Environ. Res.* 214, 113905.

Mudau, M., Ngobeni-Nyambi, R., Momba, M.N.B., 2023. *Pathogens* 12, 1085.

Ndlovu, K.S., Moloto, M.J., Sekhosana, K.E., Nkambule, T.T.I., Managa, M., 2022. *Environ. Sci. Pollut. Res.* 30, 11210-11225.

Necibi, M.C., Dhiba, D., El Hajjaji, S., 2021. *Sustainability* 13, 1125.

Nieuwenhuijsen, M.J., Smith, R., Golfopoulos, S., Best, N., Bennett, J., Aggazzotti, G., Righi, E., Fantuzzi, G., Bucchini, L., Cordier, S., Villanueva, C.M., Moreno, V., Vecchia, C. La, Bosetti, C., Vartiainen, T., Rautiu, R., Toledano, M., Iszatt, N., Grazuleviciene, R., Kogevinas, M., 2009a. *J. Water Health* 7, 185–207.

Nieuwenhuijsen, M.J., Martinez, D., Grellier, J., Bennett, J., Best, N., Iszatt, N., Vrijheid, M., Toledano, M.B., 2009b. *Environ. Health Perspect.* 117, 1486–1493.

Pastorino, P., Ginebreda, A., 2021. *Int. J. Environ. Res. Public Health* 18, 13401.

Pucelik, B., Dąbrowski, J.M., 2022. Photodynamic inactivation (PDI) as a promising alternative to current pharmaceuticals for the treatment of resistant microorganisms. pp. 24, 65–108.

Sen, P., Soy, R., Mgidlana, S., Mack, J., Nyokong, T., 2022. *Dye. Pigment.* 203, 110313.

Thandu, M., Comuzzi, C., Goi, D., 2015. *Int. J. Photoenergy* 2015, 1–22.

Tsolekile, N., Parani, S., Matoetoe, M.C., Songca, S.P., Oluwafemi, O.S., 2017. *Nano-Structures & Nano-Objects* 12, 46–56.

Yadav, D., Rangabhashiyam, S., Verma, P., Singh, P., Devi, P., Kumar, P., Hussain, C.M., Gaurav, G.K., Kumar, K.S., 2021. Chemosphere 272, 129492.

CHAPTER 2

LITERATURE REVIEW

2.1 INTRODUCTION

Water is life- a meaningful phrase that regards water as a crucial element of life. As essential as is, some populations are restricted to safe and clean water sources. This can be caused by ineffective treatment of industrial waste, sewage, and pharmaceuticals in water. Which is exacerbated by emerging pollutants and antimicrobial resistance. This poses many risks and challenges in water treatment due to limited understanding and effective removal methods. Effective techniques and continuous studies are crucial to eliminate these complex issues.

2.1.1 THE WATER TREATMENT PROCESS

The commonly used domestic wastewater treatment process in South Africa is shown in **Figure 2.1** (Genevieve Harding et al., 2020). Removal of large objects that could damage plant equipment is carried out in the first stage known as bar filtration. Further steps include removal of fine particles and separation of solid organic matter from the inflow. Aeration is then conducted to encourage the formation of NO_3^- from NH_3 and increase the oxygen concentration for bacterial growth. The role of bacteria is to remove oxygen molecules from nitrate to produce nitrogen gas (Wall, 2018). As the bacterial count increases due to aeration, sterilization is very important in the next step. Chlorination, ozonation and ultraviolet sterilization are common sterilization techniques applied in this step, which is applied after the water being treated passes through the secondary clarifier (Schoeman et al., 2017). Finally, water analysis takes place before redistributed back to the water system for consumption.

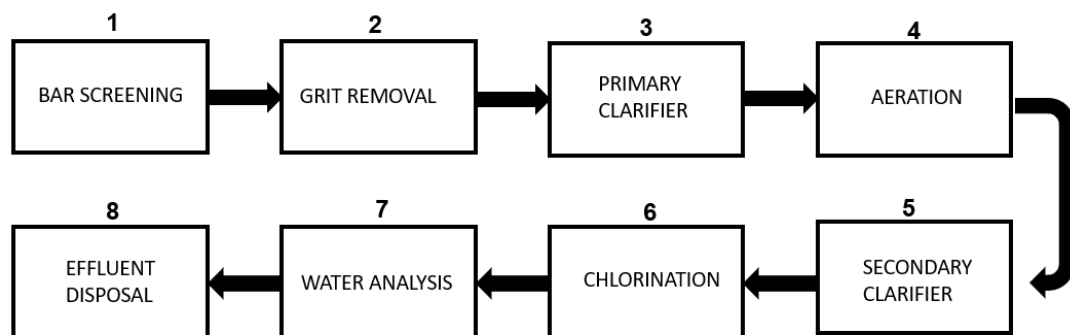


Figure 2.1. Commonly used wastewater treatment process in South Africa, outlining chlorination as the common sterilization technique.

DBPs such as THMs are common when chlorination is the implemented disinfection technique in water containing organic matter (Gallard and von Gunten, 2002). THMs are regulated by the South African National Standard (SANS) 241 for drinking water. However, this standard has high acceptable levels of THMs when compared to other regions of the world, and rather experience relatively high cancer cases related to THMs (Ololade et al., 2019). This means South Africans are at a much greater risk and exposure to THMs cancer related cases. Factors influencing the concentration of THMs include the concentration of organic matter, amount of chlorine used for disinfection, contact time between chlorine and organic matter, and lastly the water temperature (Allard et al., 2015). Hence, to attain the least concentration of THMs in treated water, it is vital to optimize the treatment process by utilizing appropriate amount of chlorine and minimizing the contact time between chlorine and natural matter. Moreover, keeping the water temperature low can decrease of THM formation.

In South Africa, ozonation and ultraviolet (UV) sterilization are rarely used, while chlorination is preferred (Jalali Milani and Nabi Bidhendi, 2022). Ozonation and UV radiation have been shown to be effective in inactivating most forms of bacteria with few adverse results. However, some problems still exist regarding the application of UV radiation to the purification process. This includes reversing the UV effect by correcting dark, ineffective low doses, radiation duration and turbidity in treated wastewater (Lanrewaju et al., 2022). However, these problems do not exist in the presence of photosensitizers (PSs) and semiconductor nanoparticles such as QDs.

2.1.2 MICROBES IN WATER TREATMENT

Microorganisms are microscopic organisms that can be seen under a microscope. A small fraction of these bacteria are infectious and can accumulate in the human body consequently causing a disease (Alderson and Rowland, 1995). Common sources of infectious bacteria include drinking contaminated water, contaminated food or direct contact with the excrement of an infected person or animal.

Although wastewater disinfection is considered effective, some bacteria mutate and develop resistance to certain treatment methods. Mutant bacteria cause more severe

infections that require complex treatment and expensive initial diagnosis (Parandhaman et al., 2015). The findings of Ridgway and Olson showed that different bacterial strains have different sensitivity to chlorine (Ridgway and Olson, 1982). Bacteria obtained from chlorinated water pipes have been found to have relative immunity to both combined and free chlorine compared with bacteria from untreated pipes. This suggests the existence of more chlorine resistant bacteria in chlorinated water systems (Ridgway and Olson, 1982). The goal of disinfection is to eradicate bacteria so that humans and animals are protected from infection. This is not fully achieved by chlorination as some strains can still survive.

Chlorination is effective in preventing outbreaks of waterborne diseases, but it also encourages the exchange of antibiotic resistance genes (ARGs) between different groups of bacteria through natural selection (Jin et al., 2020). Jin et al., recently studied ARGs caused by antibiotic-resistant bacteria (ARBs) being destroyed and producing bacteria damaged by the chlorine released by chlorination. The objective of the study was to investigate their effects on the horizontal transport of ARGs during chlorination. The results showed that *E. faecalis*, *E. coli* and *P. aeruginosa* have different immunity to sodium hypochlorite, a compound used for chlorination (Jin et al., 2020).

Transmissible plasmid RP4 (IncP alpha) can be continuously emitted from annihilated donors. Subsequent water standards are regulated by chemical oxygen demand, metal ions and ammonium which can assist the rate of conversion of RP4 to damaged *E. faecalis* bacteria. The situation, therefore, presents a potential health risk (LeChevallier et al., 1988). In addition, bacteria adherence to surfaces contributes the most to disinfection resistance. Biofilm age, encapsulating bacteria and past-growth conditions are also factors that increase chlorine resistance.

2.1.3 TYPES OF BACTERIA

Bacteria can be classified into two groups; they are either gram-negative or gram-positive. Gram-positive bacteria consist of a thicker sheet of peptidoglycan in their cytoplasmic wall, while gram-negative bacteria have a thinner plate (Mai-Prochnow et al., 2016). Gram-positive bacteria also lack the outer lipopolysaccharide membrane that gram-negative bacteria possess in the outer membrane, contributing to differences in susceptibility to antibacterial agents (**Figure 2.2**). Thus, the thinnest

layer of gram-negative bacteria is likely to be penetrated by antibacterial nanoparticles during ROS generation, leading to cell destruction.

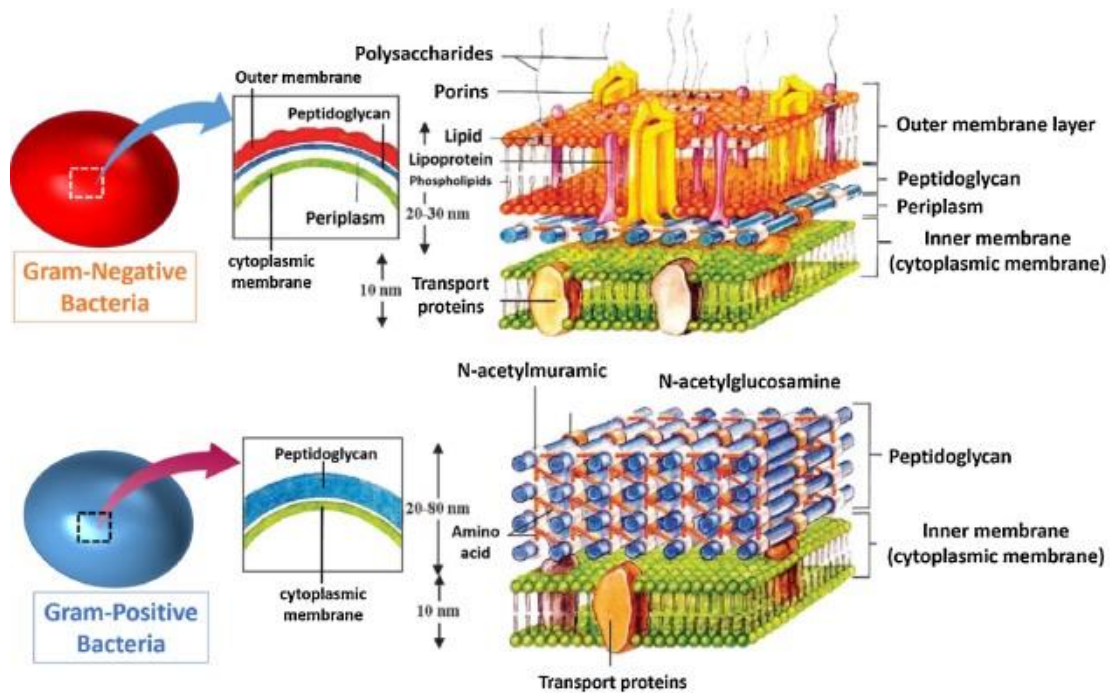


Figure 2.2. Differences between cellwall structures of gram-positive and -negative bacteria (Josset et al., 2008).

2.2 QUANTUM DOTS

Several nanoparticles have been identified to possess antimicrobial properties through their ability to transport drugs and related compounds. They provide several streams of activation including light and magnetic fields. These streams provide additional means of fighting disease-causing bacteria. Thanks to the generation of oxidizing compounds, killing of bacterial cells is accomplished (Raghupathi et al., 2011). Nanoparticles can inhibit the growth of bacteria and can be used in the treatment of sources of bacterial infection in the environment. This includes healthcare substrates, food packaging and water treatment (Simeonidis et al., 2016).

Quantum dots (QDs) are among several different nanoparticles studied for their antibacterial activity. Morphology, size and other properties contribute to the antimicrobial efficacy of nanoparticles (Zhang et al., 2019). The more spherical morphology increases the surface area, and the smaller size improves the optical

properties of the nanoparticles. The size-dependent optical properties of nanoparticles are based on changes in the optical energy bandgap, which influences the surface plasmon resonance. Especially in semiconductor nanoparticles, the optical bandgap increases as the particle size decreases. Specifically regarding the spherical morphology and small size (nm) of QDs, the necessary criteria to be a good antibacterial nanoparticle is achieved (Zhang et al., 2019). QDs can be synthesized from various precursors of semiconductor materials with desired properties. More importantly, they exhibit stable fluorescence without the use of a laser. Stable fluorescence relates to a long fluorescence lifetime that suggests fewer competing non-radiative decay pathways. QDs with longer fluorescence lifetime have low photon turnover rates, which promotes non-radiative transition. In the presence of oxygen, QDs can transfer energy to oxygen in the triple ground state to yield $^1\text{O}_2$ for bacterial photoinactivation (MacDonald and Dougherty, 2001).

The two main synthetic routes of QDs synthesis are the top-down and bottom-up approaches (Crouch et al., 2003). During top-down synthesis, the bulk material is thinned to form QDs. Some of the different techniques used in this method are electron beam lithography, reactive ion lithography, focused beam lithography and dip pen lithography (Green, 2002). Some of the limitations of this method are structural imperfections caused by patterning and impurities in the QDs. In a bottom-up approach, different chemical and physical methods are exploited to form nanoparticles and clusters (Shi et al., 2019). Physical methods include molecular beam epitaxial growth, colloidal synthesis and physical/chemical vapor deposition techniques (Crouch et al., 2003).

Table 2.1 describes the antibacterial mechanisms of QDs that have been studied previously in different bacteria. The data suggest that QDs are good photoinactivators of bacteria. Under irradiation of appropriate wavelength, cytotoxic ROS against bacteria are generated by QDs (Anand et al., 2020). This led to sudden interest in the antibacterial mechanisms of QDs and has been simplified as shown in **Figure 2.3**. The effectiveness of inhibitory activity is mainly influenced by ligand, zeta potential, size, shape and charge transfer effect (Rajendiran et al., 2019).

Table 2.1. Antibacterial mechanisms of QDs that have been studied previously in different bacteria.

Quantum dots (QDs)	Microbe	Antibacterial mechanism	References
CdTe QDs (5-10 nm)	<i>Escherichia coli</i>	Induce membrane stress	(Lu et al., 2008)
ZnO QDs (3-7 nm)	<i>Escherichia coli</i>	Generate reactive oxygen species (ROS)	(Joshi et al., 2009)
CdSe QDs (7 nm)	<i>Pseudomonas aeruginosa</i> ,	Induce cell and genomic toxicity	(Priester et al., 2009)
CdS/Ag ₂ S QDs (2-19 nm)	<i>Escherichia coli</i> , <i>Pseudomonas aeruginosa</i> , <i>Staphylococcus aureus</i>	DNA structure damage and penetration of the cell wall	(Neelgund et al., 2012)

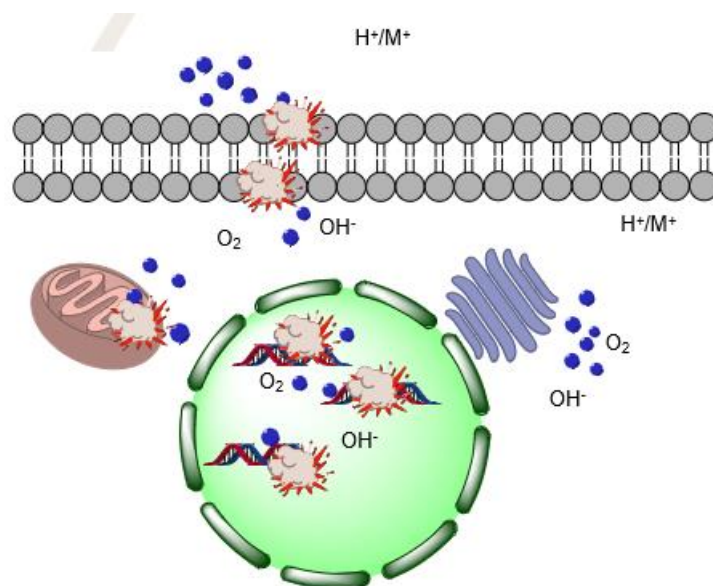


Figure 2.3. Simplified antibacterial mechanism for quantum dots (Rajendiran et al., 2019).

2.3 PORPHYRINS

Porphyrins are heterocyclic organic compounds consisting of 4 variable pyrrole components that are coordinated to their alpha carbon atoms via a methine bridge

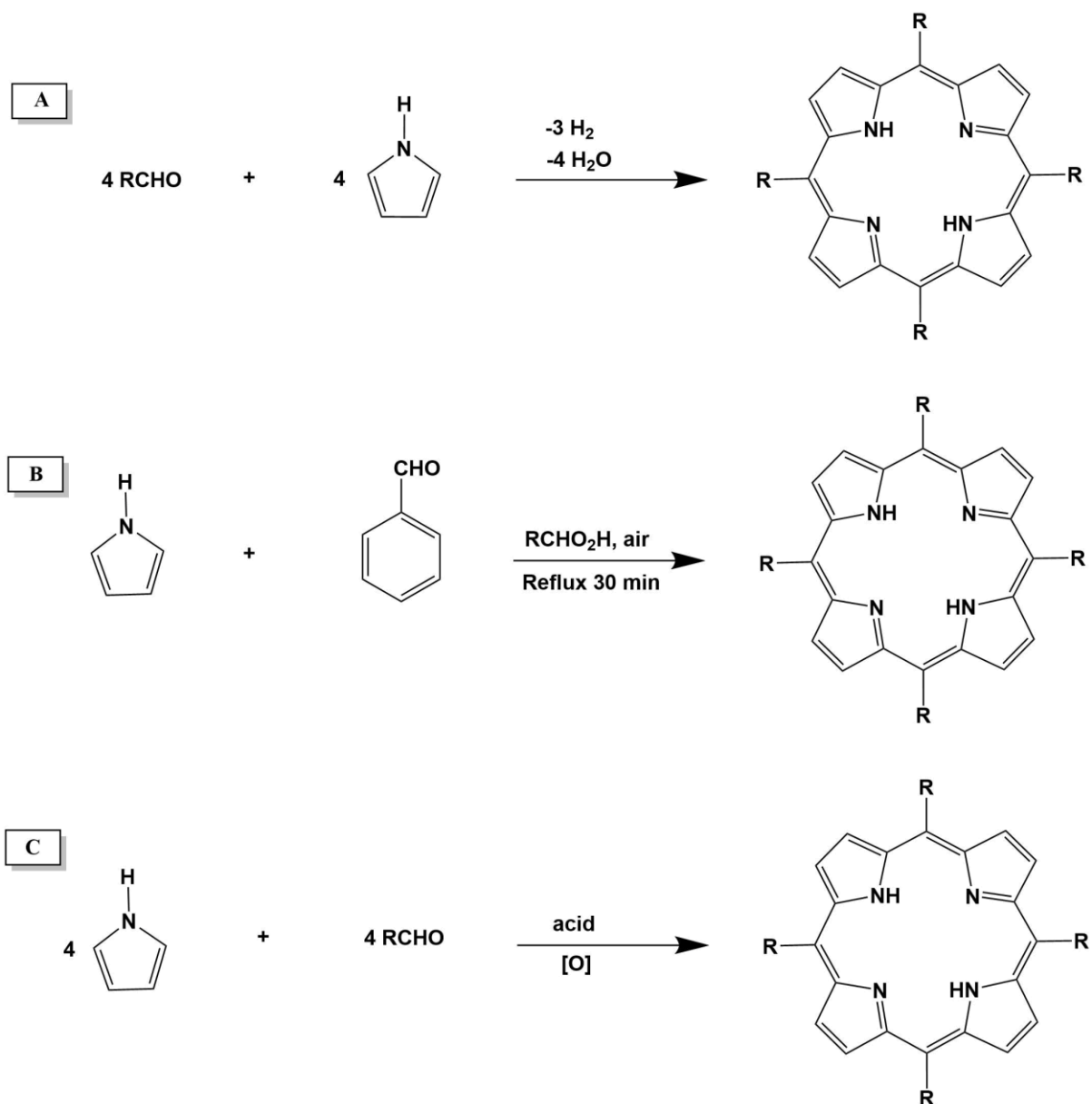
(Rayati and Malekmohammadi, 2016). They act as a photosensitizer (PS) and play an important role in photodynamic activity against bacteria. This occurs through photocatalysis of the photosensitive agent, which is key to antibacterial inactivation.

2.3.1 SYNTHETIC ROUTES OF PORPHYRINS

Several synthetic routes of porphyrins have been reported, as well as further chemical changes that improve desired characteristics for application. Rothemund and Menotti (Rothemund's method) obtained a 10% yield by reacting pyrrole and benzaldehyde in pyridine at 220 °C for a day (**Scheme 2.1 A**) (Reddi et al., 2002). Alder-Longo's method was later reported to yield 20% of a porphyrin by modifying Rothemund's method (**Scheme 2.1 B**). This involved a decrease of the reaction temperature and shorter refluxing periods. Pyrrole and benzaldehyde were refluxed in propionic acid for the mentioned reaction (Merchat et al., 1996).

Lindsey et al. 1986 further reported the use of acid-unstable aldehydes to modify the Alder-Longo method (**Scheme 2.1 C**) (Kee et al., 2008). The modification involved the incorporation of trifluoroacetic acid or $\text{BF}_3 \cdot \text{OEt}_2$ as catalysts for 1 h (Ergaieg and Seux, 2009). This method can yield significant products. However, environmentally friendly synthetic routes are promising to replace conventional synthetic routes. These routes include microwave-assisted synthesis, ionic liquids as solvents, none-solvent reactions and solid acid catalysts (Orlandi et al., 2013).

Progressive innovation has resulted in the employment of microwave irradiation for synthesis of meso-substituted porphyrins. Zerrouki et al. 1996 proposed and utilized a dual-step procedure to synthesize meso-tetraphenylporphyrins under a microwave irradiation reaction media (Boëns et al., 2010). A yield of ~47% was obtained in less than 30 min by reacting dichloromethane (DCM), benzaldehyde and pyrrole in a solution of diluted iodide. Further studies also achieved relatively high yields in shorter reaction time and less reactants by using the microwave-assisted procedure (Naik et al., 2003; Nia et al., 2010).



Scheme 2.1. General synthetic routes of porphyrins (Reddi et al., 2002, Merchat et al., 1996, Kee et al., 2008).

2.3.2 METALATION

Porphyrin metalation is the coordination of a metal ion into a porphyrin molecule, forming a metalloporphyrin (Shubina et al., 2007). Metalation is important in bioinorganic chemistry associated with active sites of heme proteins. It brings enhanced catalytic activity, biological significance, sensor applications and photophysical properties. Metalation can also modulate the electronic structure of porphyrins, improving their optical and redox properties. A study of *in vitro*

photoinactivation of *E. coli* using cationic 5,10,15,20-tetra(pyridin-3-yl) porphyrin and Zn(II) derivative conjugated to graphene quantum dots attests the latter. The metalated derivative possessed a higher Φ_{Δ} at 0.69 with a log reduction of 9.42, compared to a low Φ_{Δ} at 0.28 with a log reduction of 0.94 for the un-metalated derivative (**Figure 2.4**).

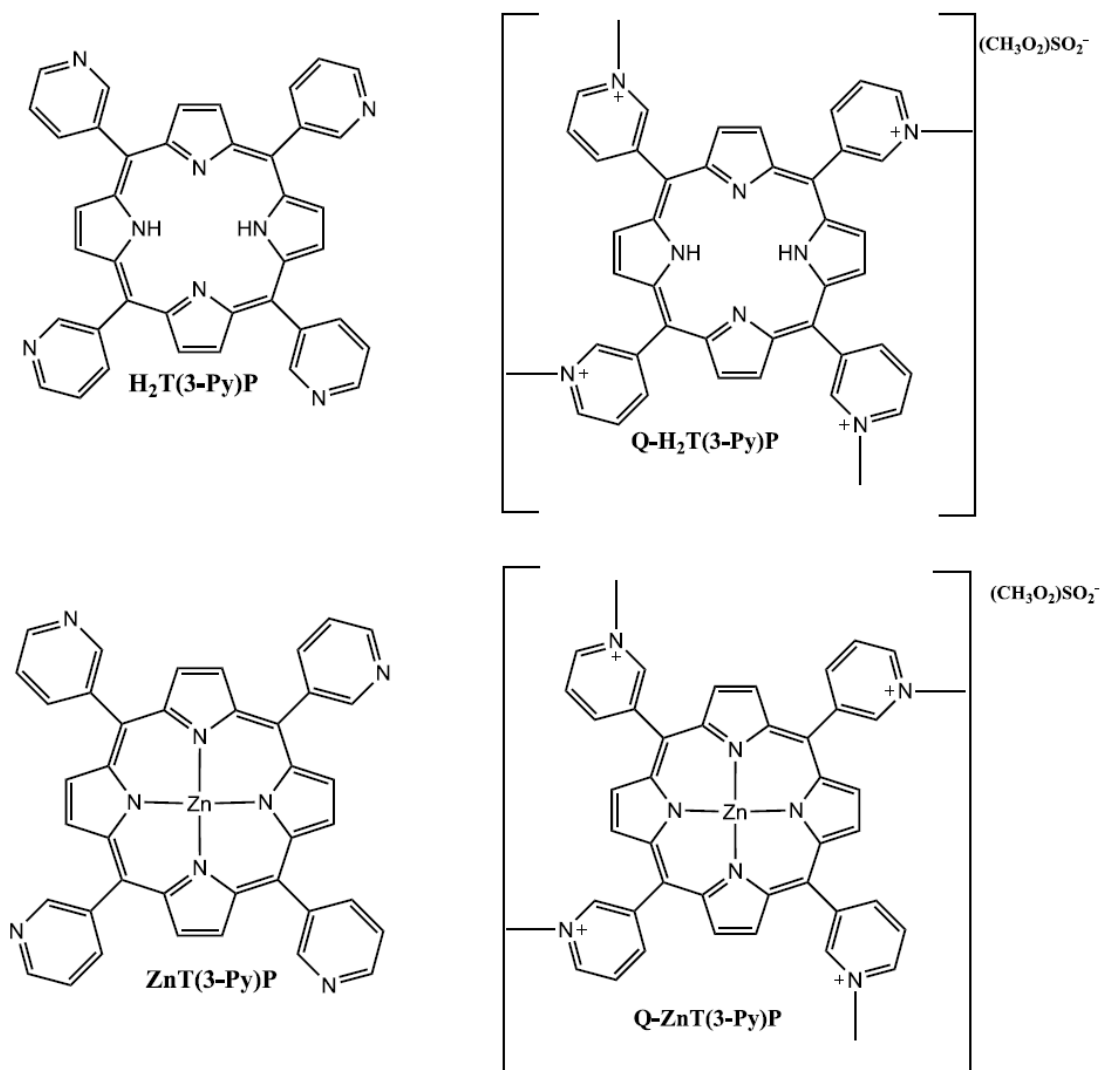


Figure 2.4. Molecular structures of 5,10,15,20-tetra(pyridin-3-yl) porphyrin, Zn 5,10,15,20-tetra(pyridin-3-yl) porphyrin and quaternized derivatives.

2.3.3 PHOTOSENSITIZATION

One technique that shows the potential to aid conventional sterilization methods include photocatalytic sterilization. This technique requires three main factors for application in the environment: photosensitizer, light absorption and oxygen (O_2)

(Thandu et al., 2015). Photosensitive substances used to disinfect water include synthetic dyes such as methylthioninium chloride and porphyrinoids. These organic catalysts can kill bacteria through the production of ROS upon light irradiation. When irradiated at the appropriate wavelength, ROS are produced when the photosensitive substance transfers energy to O_2 . These ROS can induce cytotoxic effects in undesirable bacteria and oxidize organic pollutants to CO_2 and water (Memar et al., 2018). This phenomenon occurs through either type 1 or type 2 mechanisms, but both mechanisms can occur under other circumstances. The type 1 mechanism involves the transfer of electrons from the excited photosensitizer to another molecule and the generation of free radicals, monovalent anion O_2^- , O_2H and OH . Reports have shown that reactions occurring through a type 1 mechanism have a notable role in the sterilization of gram-negative bacteria (Ergaieg et al., 2008).

Type 2 mechanisms involve the transfer of energy between the photosensitizer and oxygen to produce singlet oxygen species (DeRosa, 2002). A Jablonski diagram was used to show how type 1 and 2 mechanisms occur, as shown in **Figure 2.5**. Bacterial survival was significantly reduced when photocoagulation was used. Photokilling mainly occurs through two approaches as photosensitizers accumulate in bacteria. One approach involves damage to the cytoplasmic membrane and the other involves DNA disruption.

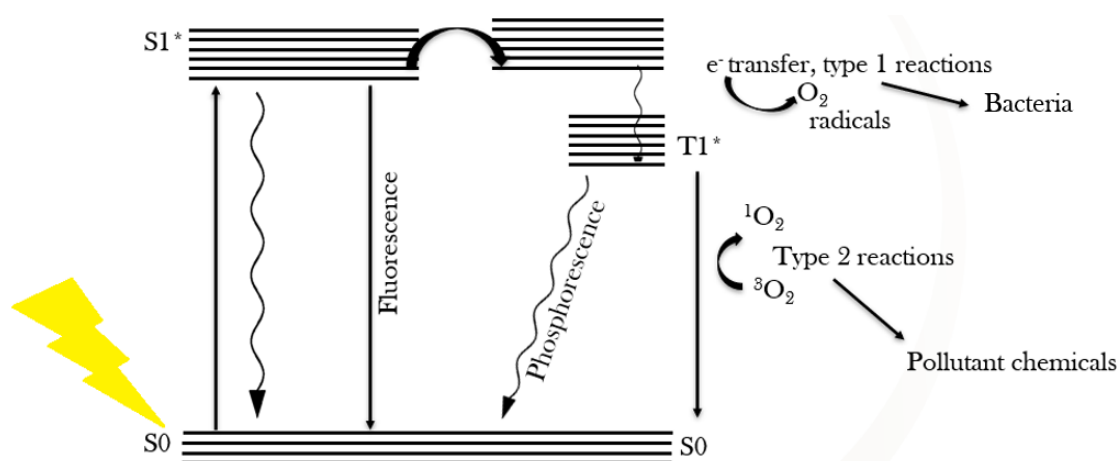


Figure 2.5. The Jablonski diagram (Jablonski, 1933).

In most cases, PSs absorb about 400-800 nm of the electromagnetic spectrum. Excitation occurs when a photon is transferred from the ground state (S_0) to the

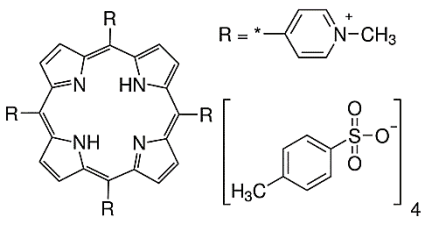
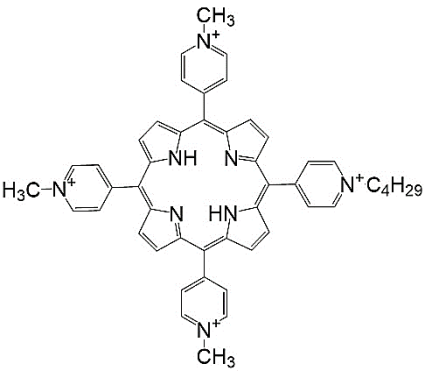
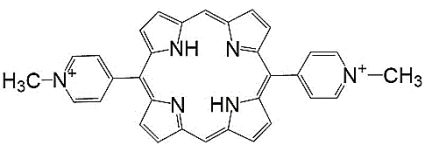
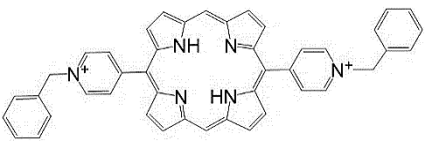
excited single group state (S1*). The triple excited state (T1*) can also occur due to inter-system interference (ISC) of (S1*). Then, fluorescence and phosphorescence will occur when the photon returns to the ground state from (S1*) and (T1*), respectively (DeRosa, 2002). Furthermore, (T1*) can transfer its energy to another molecule due to its longer lifetime. This phenomenon is called non-radiative transition. Because of the presence of oxygen, the photosensitizer can transfer energy to oxygen in the triple ground state shown by the type 2 mechanism in **Figure 2.5** to yield ¹O₂ singlet oxygen (MacDonald and Dougherty, 2001).

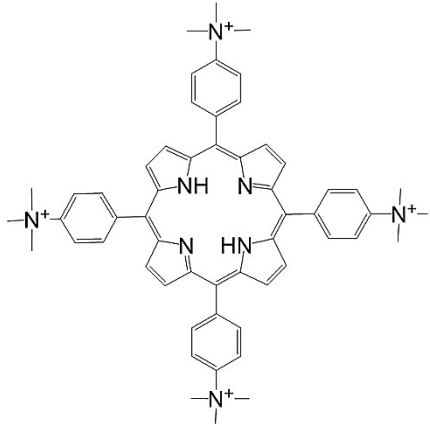
2.3.4 PHOTOINACTIVATION ACTIVITY

D. radiodurans cells are known to be radiation resistant and are the most radiation resistant bacteria in the world (Liu et al., 2023). It can withstand a radiation dose of 5 kGy during a period of stable growth without showing signs of mutation. The radiopaque ability of *D. radiodurans* is more than 30x greater than *E. coli* and more than 1000x greater than that of humans (Krisiko and Radman, 2013). These cells underwent TMPyP-mediated photoinactivation and the results showed leakage of potassium, phosphate, and magnesium from the cells. Leakage through damaged membranes is key to cell destruction. This suggests that photochemistry induces structural and functional destruction of the bacteria to successfully destroy it (Lopes et al., 2014).

The photodynamic effect of TMPyP was also tested on different *E. Coli* bacterial cell lines and cell survival was reduced by 5 log after 30 min of illumination. Protein-protein cross-linking of the cytoplasmic membrane of *S. aureus* is also altered by photochemistry and causes changes in plasmid and chromosomal DNA. This resulted in the inactivation of *S. aureus* cells by photochemistry. **Table 2.2** shows that many porphyrins significantly reduce bacteria when used in photochemical killing (Magaraggia et al., 2006).

Table 2.2. Porphyrins used for photochemistry of different bacteria and their reduction efficiency.

Porphyrins	Microbes	Reduction	References
 <p><i>meso</i>-tetra (4-<i>N</i>-methyl-4-pyridyl) porphyrin tetra-tosylate (TMPyP)</p>	<i>E. hirae</i> , <i>E. coli</i>	7.5-log	(Ergaieg and Seux, 2009)
 <p>Tri-meso(<i>N</i>-methyl-pyridinium), meso(<i>N</i>-tetradecyl-pyridinium) porphine (Tri-Py⁺-Me-PyTD)</p>	<i>S. aureus</i> , <i>E. coli</i>	7-log, 6-log, respectively	(Magaraggia et al., 2006)
 <p>5,15-Di(<i>N</i>-methyl-4-pyridinium) porphyrin (DMPyP)</p>	<i>E. faecalis</i>	6-log	(Orlandi et al., 2013)
 <p>5,15-Di(<i>N</i>-benzyl-4-pyridinium) porphyrin (DBPyP)</p>	<i>E. faecalis</i> , <i>E. coli</i>	6-log	(Orlandi et al., 2013)

 <p>5,10,15,20-tetrakis (4-N,N,N-trimethylanilinium) porphyrin (TMAP⁴⁺)</p>	<i>E. seriolicida</i>	7-log	(Merchat et al., 1996)
---	-----------------------	-------	------------------------

2.4 REFERENCES

- Alderson, P., Rowland, M., 1995. Microorganisms, in: Making Use of Biology. Macmillan Education UK, London.67, 17–32.
- Allard, S., Tan, J., Joll, C.A., von Gunten, U., 2015. Environ. Sci. Technol. 49, 11105–11114.
- Anand, K.V., Sandy Subala, A., Sumathi, K.S., Antony Lucia Merin, S., 2020. Eur. J. Adv. Chem. Res. 1. 68-75.
- Boëns, B., Faugeras, P.-A., Vergnaud, J., Lucas, R., Teste, K., Zerrouki, R., 2010. Tetrahedron 66, 1994–1996.
- Crouch, D., Norager, S., O'Brien, P., Park, J.-H., Pickett, N., 2003. Philos. Trans. R. Soc. London. Ser. A Math. Phys. Eng. Sci. 361, 297–310.
- DeRosa, M., 2002. Coord. Chem. Rev. 233–234, 351–371.
- Ergaieg, K., Chevanne, M., Cillard, J., Seux, R., 2008. Sol. Energy 82, 1107–1117.
- Ergaieg, K., Seux, R., 2009. Desalination 246, 353–362.
- Gallard, H., von Gunten, U., 2002. Water Res. 36, 65–74.
- Genevieve Harding, Jemitias Chivavava, Alison E Lewis, 2020. Water SA 46. 387-396.
- Green, M., 2002. Curr. Opin. Solid State Mater. Sci. 6, 355–363.
- Jablonski, A., 1933. Nature 131, 839–840.

- Jalali Milani, S., Nabi Bidhendi, G., 2022. *Int. J. Environ. Res.* 16, 9.
- Jin, M., Liu, L., Wang, D., Yang, D., Liu, W., Yin, J., Yang, Z., Wang, H., Qiu, Z., Shen, Z., Shi, D., Li, H., Guo, J., Li, J., 2020. *ISME J.* 14, 1847–1856.
- Joshi, P., Chakraborti, S., Chakrabarti, P., Haranath, D., Shanker, V., Ansari, Z.A., Singh, S.P., Gupta, V., 2009. *J. Nanosci. Nanotechnol.* 9, 6427–6433.
- Josset, S., Keller, N., Lett, M.-C., Ledoux, M.J., Keller, V., 2008. *Chem. Soc. Rev.* 37, 744.
- Kee, H.L., Bhaumik, J., Diers, J.R., Mroz, P., Hamblin, M.R., Bocian, D.F., Lindsey, J.S., Holten, D., 2008. *J. Photochem. Photobiol. A Chem.* 200, 346–355.
- Krisko, A., Radman, M., 2013. *Cold Spring Harb. Perspect. Biol.* 5, 012765–012765.
- Lanrewaju, A.A., Enitan-Folami, A.M., Sabiu, S., Swalaha, F.M., 2022. *Front. Microbiol.* 13, 11643-11668.
- LeChevallier, M.W., Cawthon, C.D., Lee, R.G., 1988. *Appl. Environ. Microbiol.* 54, 649–654.
- Liu, F., Li, N., Zhang, Y., 2023. *Radiat. Med. Prot.* 4, 70–79.
- Lopes, D., Melo, T., Santos, N., Rosa, L., Alves, E., Clara Gomes, M., Cunha, Â., Neves, M.G.P.M.S., Faustino, M.A.F., Domingues, M.R.M., Almeida, A., 2014. *J. Photochem. Photobiol. B Biol.* 141, 145–153.
- Lu, Z., Li, C.M., Bao, H., Qiao, Y., Toh, Y., Yang, X., 2008. *Langmuir* 24, 5445–5452.
- MacDonald, I.J., Dougherty, T.J., 2001. *J. Porphyr. Phthalocyanines* 05, 105–129.
- Magaraggia, M., Faccenda, F., Gandolfi, A., Jori, G., 2006. *J. Environ. Monit.* 8, 923.
- Mai-Prochnow, A., Clauson, M., Hong, J., Murphy, A.B., 2016. *Sci. Rep.* 6, 38610.
- Memar, M.Y., Ghotaslou, R., Samiei, M., Adibkia, K., 2018. *Infect. Drug Resist.* 11, 567–576.
- Merchat, M., Bertolini, G., Giacomini, P., Villaneuva, A., Jori, G., 1996. *J. Photochem. Photobiol. B Biol.* 32, 153–157.
- Naik, R., Joshi, P., Kaiwar (nee Vakil), S.P., Deshpande, R.K., 2003. *Tetrahedron* 59, 2207–2213.
- Neelgund, G.M., Oki, A., Luo, Z., 2012. *Colloids Surfaces B Biointerfaces* 100, 215–221.
- Nia, S., Gong, X., Drain, C.M., Jurow, M., Rizvi, W., Qureshy, M., 2010. *J. Porphyr. Phthalocyanines* 14, 621–629.
- Ololade, O.O., Mavimbela, S., Oke, S.A., Makhadi, R., 2019. *Sustainability* 11, 4238.
- Orlandi, V.T., Caruso, E., Tettamanti, G., Banfi, S., Barbieri, P., 2013. *J. Photochem. Photobiol. B Biol.* 127, 123–132.

- Parandhaman, T., Das, A., Ramalingam, B., Samanta, D., Sastry, T.P., Mandal, A.B., Das, S.K., 2015. *J. Hazard. Mater.* 290, 117–126.
- Priester, J.H., Stoimenov, P.K., Mielke, R.E., Webb, S.M., Ehrhardt, C., Zhang, J.P., Stucky, G.D., Holden, P.A., 2009. *Environ. Sci. Technol.* 43, 2589–2594.
- Raghupathi, K.R., Koodali, R.T., Manna, A.C., 2011. *Langmuir* 27, 4020–4028.
- Rajendiran, K., Zhao, Z., Pei, D.-S., Fu, A., 2019. *Polymers (Basel)*. 11, 1670.
- Rayati, S., Malekmohammadi, S., 2016. *J. Exp. Nanosci.* 11, 872–883.
- Reddi, E., Ceccon, M., Valduga, G., Jori, G., Bommer, J.C., Elisei, F., Latterini, L., Mazzucato, U., 2002. *Photochem. Photobiol.* 75, 462.
- Ridgway, H.F., Olson, B.H., 1982. *Appl. Environ. Microbiol.* 44, 972–987.
- Schoeman, C., Dlamini, M., Okonkwo, O.J., 2017. *Emerg. Contam.* 3, 95–106.
- Shi, M., Dong, L., Zheng, S., Hou, P., Cai, L., Zhao, M., Zhang, X., Wang, Q., Li, J., Xu, K., 2019. *Biochem. Biophys. Res. Commun.* 516, 1090–1096.
- Shubina, T.E., Marbach, H., Flechtner, K., Kretschmann, A., Jux, N., Buchner, F., Steinrück, H.-P., Clark, T., Gottfried, J.M., 2007. *J. Am. Chem. Soc.* 129, 9476–9483.
- Simeonidis, K., Mourdikoudis, S., Kaprara, E., Mitrakas, M., Polavarapu, L., 2016. *Environ. Sci. Water Res. Technol.* 2, 43–70.
- Thandu, M., Comuzzi, C., Goi, D., 2015. *Int. J. Photoenergy* 2015, 1–22.
- Wall, K., 2018. *J. Transdiscipl. Res. South. Africa* 14, 345-386.
- Zhang, Zhang, Liu, 2019. *Polymers (Basel)*. 11, 708.

CHAPTER 3

EXPERIMENTAL METHODOLOGY

3.1 INTRODUCTION

The experimental procedures followed to attain the objectives of this study are dispensed in this chapter. Materials, methods of synthesis, instrumentations, successful and unsuccessful attempts are discussed.

3.2 MATERIALS, REAGENTS AND SOLVENTS

The following chemicals were procured from Sigma-Aldrich, South Africa and utilized in this study: Oleylamine (Oam, 80-90%), n-hexane (ACS reagent, $\geq 98.5\%$), acetone (ACS reagent, $\geq 99.5\%$), chloroform (ACS reagent, $\geq 99.8\%$), methanol (MeOH, ACS reagent, $\geq 99.8\%$), ethanol (ACS reagent, $\geq 96\%$), 1-octadecene (ODE, 90%), indium acetate ($\text{In}(\text{Oac})_3$, 99.99%), zincstearate (ZnSt_2 , 86-87.5%), dimethylformamide (DMF, ACS reagent, $\geq 99\%$), 1-dodecanethiol (DDT, 98%), cuprous acetate ($\text{Cu}(\text{Oac})$, 99%), oleic acid (OA, analytical reagent), sodium hydroxide (NaOH, reagent grade, 97%, powder), 6-Mercapto-1-hexanol (MCH, 97%), 4-carboxybenzaldehyde (99%), benzaldehyde (reagent plus, $\geq 99\%$), propionic acid (ACS reagent, $\geq 99.5\%$), pyrrole (reagent grade, 98%), dichloromethane (DCM, ACS reagent, $\geq 99\%$), silica gel (technical grade, 40-63 μm particle size), triblock copolymer pluronic F127, sodium dioctyl sulfosuccinate (AOT, $\geq 97\%$), sulfuric acid (H_2SO_4 , ACS reagent, 95-98%), 1,3,5-trimethylbenzene (TMB, analytical standard), tetraethyl orthosilicate (TEOS, reagent grade, 98%), 3-aminopropyltriethoxysilane (APTES, 99%), N,N dicyclohexylcarbodiimide (DCC, 99%), bio-beads s-X1, 500 mL Duran Schott glass bottles, 0.45 μm micropore cellulose membrane (Merck Millipore), mannitol salt agar and nutrient agar. Millipore water was collected from iNanoWS, UNISA, Florida Campus. Phosphate buffer saline (10 mM PBS) pH 7.4 was prepared using appropriate amounts of Na_2HPO_4 and NaOH.

3.3 INSTRUMENTATION

- Ultraviolet-visible optical absorption spectroscopy was recorded using a **Lambda 650S UV/vis spectrophotometer** supplied by PerkinElmer. A 10 mm

path length quartz cuvette was used for analysis with a wavelength range of 300-800 nm.

- **Fourier transform infrared** (FT-IR) was studied using a Frontier FTIR spectrometer supplied by PerkinElmer, South Africa. Frequency scale was internally calibrated to 0.01 cm^{-1} with a He-Ne laser and the noise was reduced by signal averaging 16 scans. The analysis range was $500\text{-}4000\text{ cm}^{-1}$ and the samples were in solid state.
- **TGA 5500** supplied by Advanced Laboratory Solutions was utilized to measure the % mass loss over time with an increase in temperature. This analysis is crucial in determining the thermal stability of synthesized nanoconjugates. The thermograms were obtained from accurately weighed samples, $25\text{-}900\text{ }^{\circ}\text{C}$ temperature range, at $3\text{ }^{\circ}\text{C}$ per minute under inert conditions.
- A **QuantaChrome Autosorb IQ3** from Anton Paar was used for determination of mesopore volume by N_2 adsorption or desorption isotherms at 77 K . Prior to each measurement, degassing was carried at $100\text{ }^{\circ}\text{C}$ overnight.
- **Proton Nuclear Magnetic Resonance** (^1H NMR) spectra were analyzed using Bruker EMX 400MHz NMR spectrometer. The spectra were recorded at room temperature using DMSO-d_6 . ^1H NMR was obtained at 16 scans per sample.
- **Mass spectrometry**, A $5\text{ }\mu\text{L}$ of the sample was injected into the Dionex Ultimate 3000 UHPLC system (Thermo Scientific, Dionex, Sunnyvale, California, USA) and run through a loop for one minute at 50 % Solvent A consisting of 0.1 % formic acid in H_2O (v/v) and 50 % solvent B consisting of 0.1 % formic acid in Acetonitrile (v/v) at a flowrate of 0.3 mL/min . Mass spectra were recorded on a Bruker Compact Q-TOF mass spectrometer (Bruker Daltonics, Bremen, Germany).
- **Dynamic light scattering** (DLS) was used to deduce particle size distribution and zeta potential of quantum dots and nanoconjugates using a **Malvern Zetasizer nanoseries** by Micron Scientific.
- **Hettich Zentrifugen universal 320 R** supplied by labotec was used for precipitate separation and extraction.
- Nutritional broth, nutrient agar, phosphate buffer, and other miscellaneous apparatus were sterilized and autoclaved using the **autoclave RAU-530D**.
- **Scanning electron microscopy** (SEM) was used to acquire secondary electron images (SE), backscattered electron images (BE) and Energy

Dispersive Spectroscopic (EDS) data in high vacuum on a **JSM-IT300 Joel**. Tescan Vega 2 Scanning Electron Microscope with a W- filament. The data was used to determine the crystallinity, morphology, and elemental analysis of quantum dots and nanoconjugates. The samples were applied on a double-sided carbon tape and coated with a 5 nm gold layer to prevent charging of the surface during analysis. Images were captured at 10 kV to obtain the highest possible surface resolution with WD at 12.6, 12.8 and 12.9 mm.

- X-ray Diffractograms (XRD) were obtained from **Rigaku SmartLab X-ray Diffractometer** at the College of Science, Engineering and Technology, in the department of Physics of the University of South Africa. The data was recorded over a $2\theta = 5-80^\circ$ range on a silicon wafer slide acting as a sample holder. The reported data was processed via baseline correction of the curved background.
- Utilizing a **time correlated single photon counting system (TCSPC)**, Fluo Time 200, Picoquant GmbH, with a diode laser as the excitation source powered by PDL 425 nm, fluorescence lifetimes and fluorescence emission spectra were studied. With integrated electronics (PicoHarp 300E, Picoquant GmbH) and a peltier-cooled photomultiplier tube (PMA-C 192-N-M, Picoquant GmbH), fluorescence was detected under the magic angle. The appropriate measured emission wavelength was chosen using a monochromator with a spectral width of roughly 4 nm. The system's response function had a full width at half-maximum (FWHM) of roughly 300 ns and was measured using a scattering Ludox solution (DuPont). To provide accurate data, the ratio of stop to start pulses was kept low (below 0.05). The maxima of the emission peak were used to estimate the luminescence decay curves in all cases. Utilizing the FluoFit tool from Picoquant GmbH, the data were analyzed. The support plane method was employed to calculate the decay times' errors.
- A **Spectra-Physics Quanta Ray Indi-40-10** (118 mJ @ 355 nm, 7 ns, 10 Hz) Nd:YAG laser was used to pump a Spectra-Physics primoScan OPO (4052855 nm, 39 mJ @ 430 nm) for photo-irradiations for singlet oxygen experiments. In comparison to ZnTPP as a reference, the irradiation was carried out at the sample's crossover wavelengths (425 nm and 420 nm for POR(H₂), POR(In), and POR(H₂)-CIS/ZnS QDs-Silica, respectively). A Shimadzu UV-2550 spectrophotometer was used to monitor the breakdown of the singlet oxygen quencher.

- A **Varian Eclipse spectrofluorometer** was used to record the excitation and emission spectra of fluorescence. Excitation in the Soret band (where the standard and complex spectra overlap) and emission spectra captured between 500 and 800 nm.
- **Singlet oxygen quantum** yields were performed using Spectra-PhysicsR primoScan OPO series, driven by Spectra-Physics Quanta Ray INDI lab with a maximum pump energy of 750 mJ and output energy of 27 mJ.
- **LEDETECT 96** colony counter from LABExim products was used to measure the optical density of cultured *E. coli* and *S. aureus*, and a count system connected to an Interscience for Microbiology Scan® 500 scanner was used to count the number of colonies and deduce colony forming units (CFU/mL) of the bacteria.
- **Thermostatic oven** was used for the incubation procedures for antimicrobial photodynamic inactivation.
- **PROVSM-3 Lab plus vortex** mixer was utilized to homogenize the bacteria solution.
- Metagenomic analysis of full length 16s gene amplicons were conducted at Inqaba Biotec. Samples were sequenced on the Sequel Iie system by PacBio, raw sub-reads were processed through the SMRTlink (v11.0) Circular Consensus Sequences (CCS) algorithm to produce highly accurate reads (>QV40). These highly accurate reads were then processed through v search and taxonomic information was determined based on QIMME2.

3.4 PHOTOSENSITIZER (PORPHYRIN) SYNTHESIS

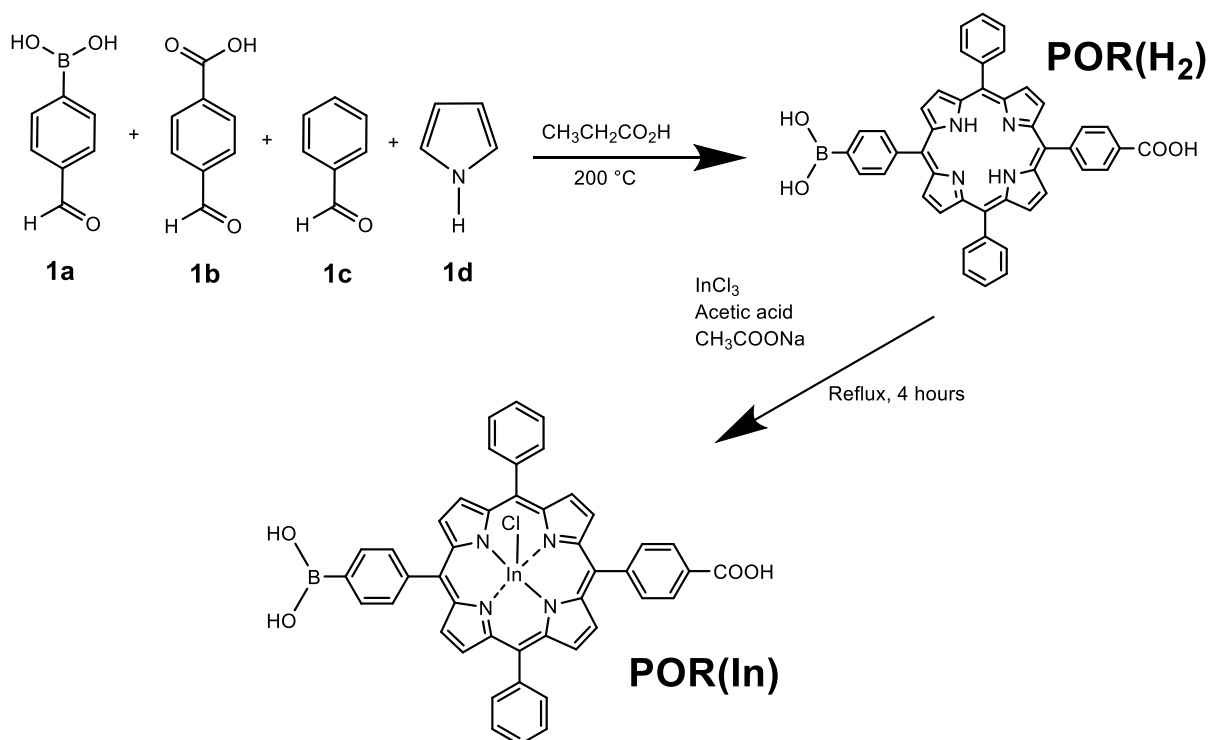
3.4.1 SYNTHESIS OF 4-(15-(4-BORONOPHENYL)-10,20-DIPHENYLPORPHYRIN-5-YL)BENZOIC ACID

With the adjustments shown in **Scheme 3.1**, Jeong et al.'s approach was used to synthesize the porphyrins used in this investigation. The metal-free derivative was created by dissolving the following ingredients in propionic acid (100 mL): **1a** (2.249 g, 0.015 mol), **1b** (2.173 g, 0.015 mol), **1c** (3.121 g, 0.031 mol), and **1d** (2.898 g, 0.043 mol). This reaction was agitated for 4 h at 200 °C. The resultant liquid was then stirred and allowed to cool to room temperature overnight. UV/vis spectroscopy and column chromatography were used to acquire pure product, once the reaction's completion

was verified. As the stationary phase, silica gel and ethyl acetate were combined, and as the mobile phase, DCM and ethyl acetate were mixed [1:1]. To choose which fraction to crystallize from, the eluted fractions from the column were compared for best UV/vis data fit. The metal-free porphyrin was precipitated with 1 M HCl, which produced a finished product that was filtered, rinsed with distilled water, and then air dried.

3.4.2 SYNTHESIS OF In(III) 4-(15-(4-BORONOPHENYL)-10,20-DIPHENYLPORPHYRIN-5-YL)BENZOIC ACID

By dissolving InCl_3 (0.442 g, 0.002 mol) and sodium acetate (0.117 g, 0.002 mol) in acetic acid (50 mL), metallization was accomplished. The mixture was then supplemented with 0.001 mol of the metal-free porphyrin, which was then refluxed for 4 h. The product was precipitated with HCl (1 M), filtered, rinsed with distilled water, and allowed to air dry.



Scheme 3.1. Synthesis of free-base and metal porphyrin.

3.5 NANOPARTICLE SYNTHESIS

3.5.1 SYNTHESIS OF $\text{CuInS}_2/\text{ZnS}$ CORE/SHELL QUANTUM DOTS

FUNCTIONALIZED WITH GLUTATHIONE

3.5.1.1 FIRST ATTEMPT

The unfavourable QDs were synthesized utilizing the solvothermal strategy (Jia et al., 2016). A Cu:In proportion of 1:2 was adopted for the synthesis. The reaction proceeded by adding 1.168g (4 mmol) of $\text{In}(\text{OAc})_3$, 0.245g (2 mmol) of $\text{Cu}(\text{OAc})_2$, 10 mL of DDT and 50 mL of octadecene in a round bottom flask. Heating then took place under N_2 flow. When the temperature reached 100 °C, 2 mL of oleic acid was added. Heating proceeded up to 220 °C and kept steady for 1 h. Fatty acids such as oleic acid and oleylamine are included to decrease accumulation of the QDs. A schematic diagram depicting the reaction setup is shown in **Figure 3.1**.

The solution was then cooled down to 120 °C by cutting off the heat supply. A zinc stock solution was then prepared and added by dissolving 1.27 g (2 mmol) of ZnSt_2 in a solution of 8 mL of octadecene and 2 mL of oleylamine at 120 °C under N_2 flow. Taking after that, the temperature was increased to a temperature extending from 240-260 °C. Aliquots of the QDs were then drawn from the solution when the temperature reached 240 °C. This continued at varying time intervals of 30 s apart, with a 5 °C increase in temperature until 260 °C was reached. However, this method was not favourable because a syringe that could be used to draw the QDs solution at high temperatures was unavailable. At 260 °C the syringes would melt and block the needle. A different method was then utilized.

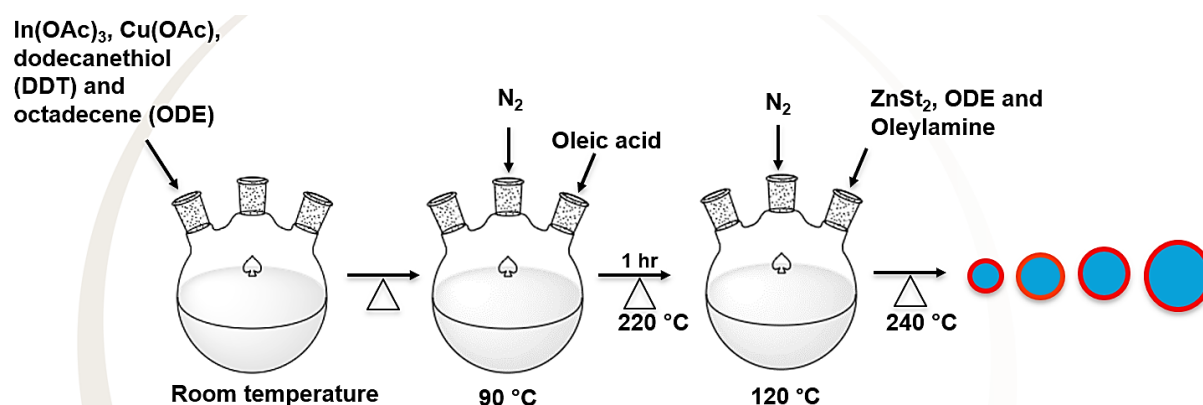


Figure 3.1. Solvothermal reaction for synthesis of $\text{CuInS}_2/\text{ZnS}$ core/shell quantum dots.

3.5.1.2 SECOND ATTEMPT

For the production of CuInS₂/ZnS QDs, a solvothermal technique was used with modifications from previously published research (Xing et al., 2009; Zikalala et al., 2020). A 1:2/3 Cu/In ratio was used, and the following procedure followed. A 100 mL Teflon-lined autoclave was filled with DDT (20 mL), In(Oac)₃ (146 mg, 0.5 mmol) and Cu(Oac)₂ (91 mg, 0.75 mmol) at room temperature (DDT was used as a sulphur source). After that, the reaction mixture was heated for 6 h at 180 °C. The Teflon-lined autoclave was cooled to room temperature after nucleation in order to produce a red product of CuInS₂ QDs.

To increase the product's stability, fluorescence capabilities, and reduce toxicity, ZnS was used as a coating reagent. Zn(Oac)₂ (367 mg, 2 mmol) was dissolved in DDT (4 mL), OA (2 mL), and ODE (8 mL) for 30 min at 160 °C to create the zinc stock solution. The solution was then transferred to the CIS core solution. The completed mixture was placed in the Teflon-lined autoclave and heated for a further 16 h at 200 °C to encourage the growth of the shell. To obtain pure CuInS₂/ZnS QDs, the mixture was repeatedly washed with acetone/chloroform (1:1) mixture.

Functionalization with glutathione (GSH) was carried out by dissolving CuInS₂/ZnS QDs (500 mg) in chloroform (5 mL) and adding GSH (200 mg, 0.65 mmol). After that, the reaction mixture was agitated for 24 h at 30 °C. The final product was precipitated with acetone, washed with distilled water and air-dried in the fume hood.

3.6 SYNTHESIS OF APTES-FUNCTIONALIZED MESOPOROUS SILICA

A modified version of APTES-functionalized mesoporous silica was synthesized from a prior study. Pluronic F127 (0.80 g), sodium dioctyl sulfosuccinate (200 mg, 0.450 mmol) and Millipore water (30 mL) were dissolved at 50 °C in a solution of H₂SO₄ (2 M). The mixture was then agitated while mesitylene (400 mg, 3.328 mmol) was added, producing a clear solution. Tetraethyl orthosilicate (3.80 g, 0.018 mol) and 3-aminopropyltriethoxysilane (300 mg, 1.673 mmol) were added thereafter, and the reaction proceeded at 50 °C for 24 h. The combination was then exposed to hydrothermal activity at 120 °C for an additional 24 h after being sealed in a 100 mL

teflon-lined autoclave. The finished product was vacuum filtered, washed with distilled water, and air-dried. A solid product was obtained and calcined at 600 °C for 6 h to get rid of the template (**Figure 3.2**).

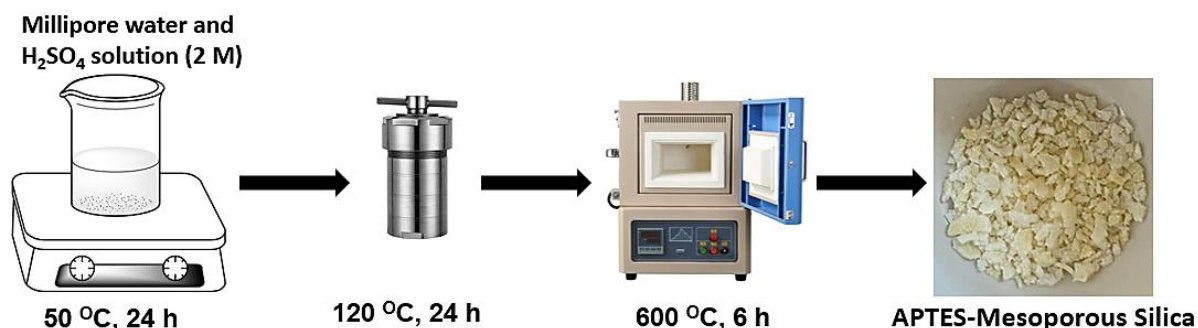


Figure 3.2. Synthetic route of APTES-mesoporous silica.

3.7 Conjugation of Porphyrin-CuInS₂/ZnS-GSH to APTES-mesoporous silica

Two steps were taken to complete this process. First, a peptide bond containing -NH₂ and -COOH groups was formed to bind POR(H₂) or POR(In) to APTES-mesoporous silica. This was done by combining DCC (0.030 g, 0.000145 mol) with POR(H₂)/POR(In) (0.025 g, 0.036 mol/0.025 g, 0.029 mol) to change the porphyrin's -COOH group into an active carbodiimide ester group. APTES-mesoporous silica (0.3 g) was then added after the mixture had been mixed for 24 h at room temperature. Then allowed to stir for an additional day. Bio-Beads S-X1 from Bio-Rad were used to separate the conjugates from the non-conjugate particles. Porphyrin-mesoporous silica was the final nanoconjugate.

The second step involved conjugating CIS/ZnS-GSH to the porphyrin-mesoporous silica nanoconjugates. This was accomplished by combining DCC (0.030 g, 0.000145 mol) with CIS/ZnS-GSH (0.5 g) to change the GSH -COOH group into an active carbodiimide ester group. POR(H₂)-/POR(In)- APTES-mesoporous silica nanoconjugate was then added after the mixture had been agitated for 24 h. This conjugation phase relies on the creation of ester bonds between the B-OH groups of the porphyrin and the GSH -COOH groups. The finished products were precipitated with acetone, centrifuged, air dried, and separated using Bio-Beads S-X1.

POR(H₂)-CIS/ZnS QDs-Silica (Metal-free derivative) and POR(In)-CIS/ZnS QDs-Silica (Metalated derivative) were the resulting nanoconjugates. **Figure 3.3** depicts the three components of POR(H₂)-CIS/ZnS QDs-Silica: **mesoporous silica**, **POR(H₂)**, and **CIS/ZnS QDs**. The conjugation/linking agents are also outlined as GSH and APTES. Conjugation of QDs and porphyrin on mesoporous silica is conducted to enable recovery and reuse of the nanoconjugate. Also, to prevent secondary contamination during the photoinactivation process. Amongst other support agents, mesoporous silica is more suitable for water and environmental applications.

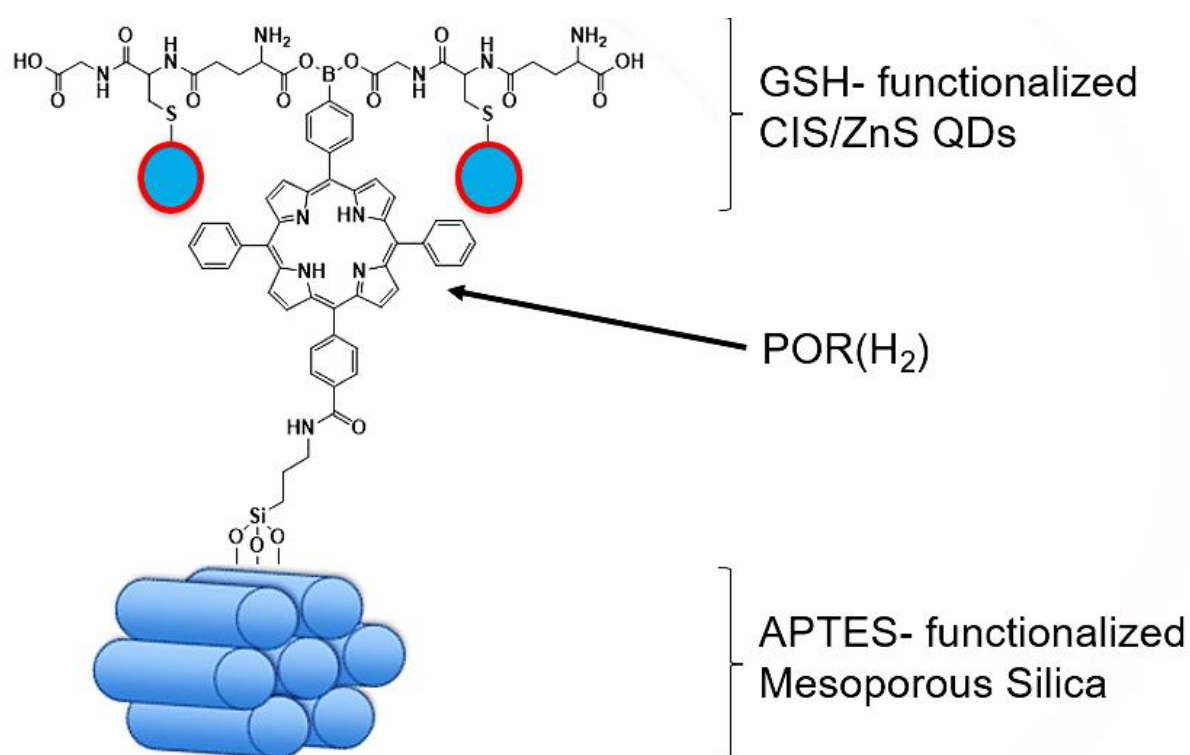


Figure 3.3. Proposed structure of nanoconjugate consisting of metal-free 4-(15-(4-boronophenyl)-10,20-diphenylporphyrin-5-yl)benzoic acid (POR(H₂)), CIS/ZnS QDs and APTES-mesoporous silica.

3.8 SAMPLING AND PREPARATION

Samples of wastewater influent were collected from Klipspruit Treatment Works, a wastewater treatment plant (GPS coordinates: 26.311433, 27.930583) located in the

province of Gauteng in South Africa. The studied water source is heavily polluted by sewage and leachate from the city's landfills. At the same sampling site, previous studies reported the presence of several antibiotics belonging to different classes such as sulfonamides, fluoroquinolones and penicillins, classified under CEC's (Ncube et al., 2021). Wastewater, collected from raw sewage discharges from neighbouring communities southeast of Johannesburg, is immediately passed through screens designed to remove large particles. This wastewater treatment plant has a treatment capacity of 200 ML/day, implementing a treatment process based on activated sludge technology. The treated wastewater is discharged into the Klip River (a tributary of the Vaal River) and is mainly used for vegetable irrigation and fishing.

Samples were collected aseptically in sterile 3x 500 mL Duran Schott glass bottles and transported immediately to the laboratory. Samples were stored in ice en-route to the laboratory for storage (transportation time no more than 1 h 30 min). Samples were then submitted for metagenomic data analysis within 24 h of collection. Remaining samples were prepared in aliquots and used for isolation of desired bacteria. Mannitol salt agar was used for the isolation of *S. aureus* and nutrient agar was used for *E. coli*.

Isolation of the bacteria was conducted via a membrane filtration unit as depicted in **Figure 3.4**. Aliquots of 100 mL were filtered through a 0.45 μm filter using a water pump. The filters were then aseptically placed on plates containing a selective media (Mulamattathil et al., 2014). The plates were then nurtured at 37 °C. **Figure 3.5** gives an overview of the bacterial growth process on a selective media.

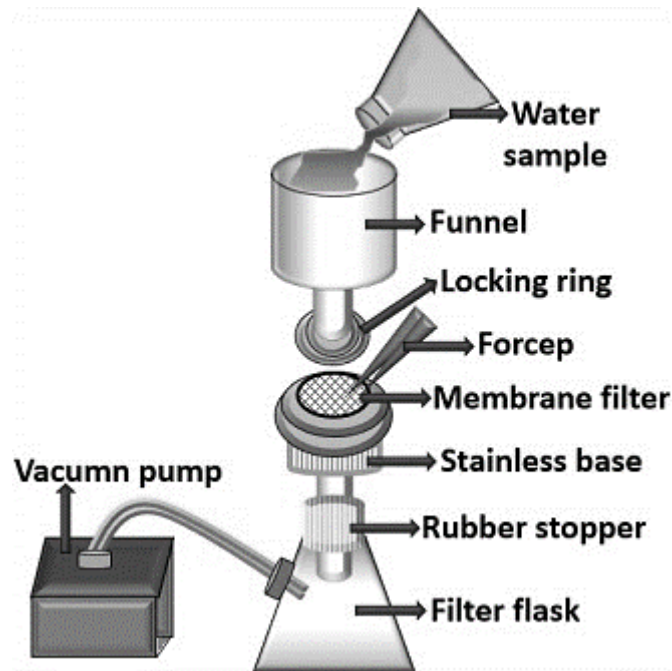


Figure 3.4. Illustration of a membrane filtration unit.

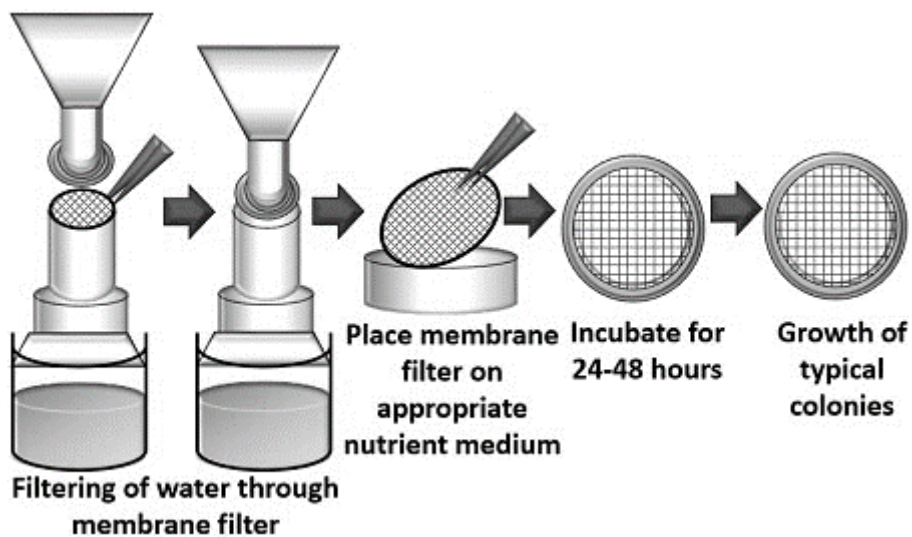


Figure 3.5. Overview of the bacterial growth process on a selective media.

3.9 DNA EXTRACTION, QUATIFICATION AND PCR AMPLIFICATION

A single colony was picked from culture media and transferred to a 2 mL tube in preparation for genomic DNA extraction. Genomic DNA was extracted using Quick-DNA™ Fungal/Bacterial Microprep Kit as per the manufacturer’s instructions. DNA was Quantified using Biodrop. Extracted DNA used for downstream PCR and sequencing analysis had $A_{260}:A_{280}$ ratios between 1.8–2.0 and DNA concentrations of 20–27 ng/μL libraries of bacterial 16S rRNA gene fragments were PCR amplified

using primer pair 27F (5'-AGAGTTTGATCCTGGCTCAG-3') and 1429R (5'-TACGGYTACCTTGTTACGACTT-3') primers. The reaction mixture of 25 μ L was comprised of 12.5 μ L master mix, 1 μ L of 0.1 μ M of both forward and reverse primer, 3 μ L of 20-27 ng/ μ L DNA and 7.5 μ L PCR water to bring the total volume to 25 μ L. The PCR parameters of the 16S are as follows initial denaturation at 95 $^{\circ}$ C for 3 min followed by 30 cycles of 95 $^{\circ}$ C for 1 min, 58 $^{\circ}$ C for 1 min and 68 $^{\circ}$ C for 2 min; and a final extension for 10 min at 72 $^{\circ}$ C. The ITS region was amplified using the following PCR conditions, initial denaturation at 95 $^{\circ}$ C for 5 min, followed by 35 cycles of 95 $^{\circ}$ C for 30 s, 55 $^{\circ}$ C for 30 s, 72 $^{\circ}$ C for 1 min and the final extension of 72 $^{\circ}$ C for 10 min. The quality and quantity of the resultant from the PCR were visualized by 1 % gel electrophoresis. One gram of agarose powder was dissolved in 100 mL of 1X TAE buffer and boiled for 3 min in the microwave, cooled and 1 μ L ethidium bromide was added. The gel was cast in an electrophoresis tray containing a sample comb to form wells and allowed to solidify. Upon solidification the gel was transferred to the electrophoresis chamber containing the 1X TAE running buffer enough to cover the gel, the comb was removed carefully to not rip the wells. The 10 kb ladder was added to determine the size of amplified DNA. DNA Samples containing PCR products were loaded into the wells and the electric voltage of 80 volts was applied to allow migration of amplified DNA sample. The DNA samples were visualized under UV transilluminator. The obtained PCR products were sequenced by Pacbio Platform at Inqaba Biotechnology (Pretoria, South Africa) according to standard protocol.

3.10 PHOTOINACTIVATION

3.10.1 NANOCONJUGATE

POR(H₂)-CIS/ZnS QDs-Silica and **POR(In)-CIS/ZnS QDs-Silica** were added to 2 % DMSO in phosphate buffer saline(PBS). A concentration of 10 μ g/mL was used for photoinactivation studies. No effect was noted on the bacteria when a control experiment was conducted. The control is when the nanoconjugates were not included in the experiment.

3.10.2 LIGHT SIMULATION

The employed photoinactivation tool was an LED-mounted irradiation chamber fitted with M415L4 LED. A radiance of $15.6 \mu\text{W}/\text{mm}^2$ was delivered onto the samples. The nanoconjugate-bacteria solutions were placed in a well microplate opposite the LED, followed by irradiation with minimal to zero external light interferences. The solutions were localized by incubating for 30 min before irradiation (Makola et al., 2020). **Figure 3.6** depicts the irradiation setup that was followed.

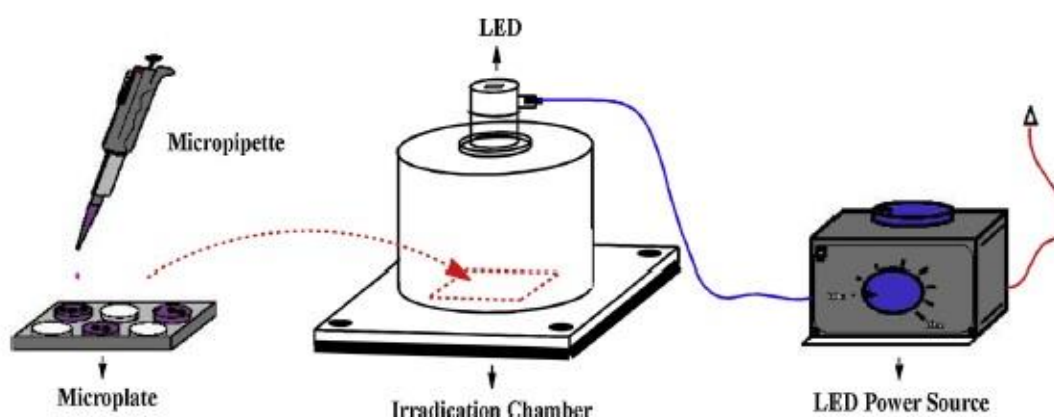


Figure 3.6. Illustration of irradiation setup using LED.

3.11 REFERENCES

- Jia, Y., Wang, H., Yan, Z., Deng, L., Dong, H., Ma, N., Sun, D., 2016. RSC Adv. 6, 93303–93308.
- Makola, L.C., Managa, M., Nyokong, T., 2020. Photodiagnosis Photodyn. Ther. 30, 101736.
- Mulamattathil, S.G., Bezuidenhout, C., Mbewe, M., Ateba, C.N., 2014. J. Pathog. 2014, 1–11.
- Ncube, S., Nuapia, Y.B., Chimuka, L., Madikizela, L.M., Etale, A., 2021. Front. Environ. Sci. 9, 1098-1132.
- Ndlovu, K.S., Moloto, M.J., Sekhosana, K.E., Nkambule, T.T.I., Managa, M., 2022. Environ. Sci. Pollut. Res. 30, 11210-11225.
- Nyokong, T., Antunes, E., 2010. Photochemical and Photophysical Properties of Metallophthalocyanines.67, 247–357.

Xing, C., Xu, Q., Tang, H., Liu, L., Wang, S., 2009. *J. Am. Chem. Soc.* 131, 13117–13124.

Zikalala, N., Parani, S., Tsolekile, N., Oluwafemi, O.S., 2020. *J. Mater. Chem. C* 8, 9329–9336.

Zoltan, T., Vargas, F., López, V., Chávez, V., Rivas, C., Ramírez, Á.H., 2015. *Spectrochim. Acta Part A Mol. Biomol. Spectrosc.* 135, 747–756.

CHAPTER 4

RESULTS AND DISCUSSIONS: CHARACTERIZATION AND PHOTO-PHYSICOCHEMICAL STUDIES

4.1 INTRODUCTION

Results from various characterization techniques and photo-physicochemical studies are provided in this chapter. This is based on the successful experimental methodology that was followed.

4.2 CHARACTERIZATION

4.2.1 Nuclear magnetic resonance (NMR), mass spectrometry (MS) and Fourier-transform infrared (FTIR) spectroscopy

The porphyrin complex was characterized by MS, ^1H -NMR and FTIR spectroscopy. MS analysis of the POR(H_2) molecular ion has a peak at $m/z = 701.8$ corresponding to $[\text{M}-\text{H}]$ (**Figure 4.1**). POR(In) showed a molecular ion peak at $m/z = 853.4$ corresponding to $[\text{M}+3\text{H}]^+$ (**Figure 4.2**). ^1H NMR were obtained for POR(H_2) and POR(In) (**Figures 4.3** and **4.4**, respectively). Pyrrolic NH is observed at -2.94 ppm for POR(H_2) but not for POR(In), indicating successful metalation of POR(H_2). The total proton count for POR(H_2) and POR(In) was H_{31} and H_{29} , respectively. ^1H NMR data obtained are consistent with the proposed structures of POR(H_2) and POR(In). FTIR spectroscopy was also used to identify the functional groups both POR(H_2) and POR(In). Both complexes had an aromatic $-\text{C}-\text{H}$ peak at 2850 to 2921 cm^{-1} , followed by a $\text{C}-\text{N}$ peak at 1581 cm^{-1} and a $\text{B}-\text{C}$ peak at 1012 cm^{-1} . $\text{C}-\text{O}$ stretches were also observed around 1102 cm^{-1} for both porphyrin complexes. Remarkably, stretching of OH is observed (**Figure 4.5**). This is wider at her POR(H_2) than at POR(In), suggesting the presence of NH at POR(H_2) rather than at POR(In). The overall characterization data were satisfactory for the compounds synthesized.

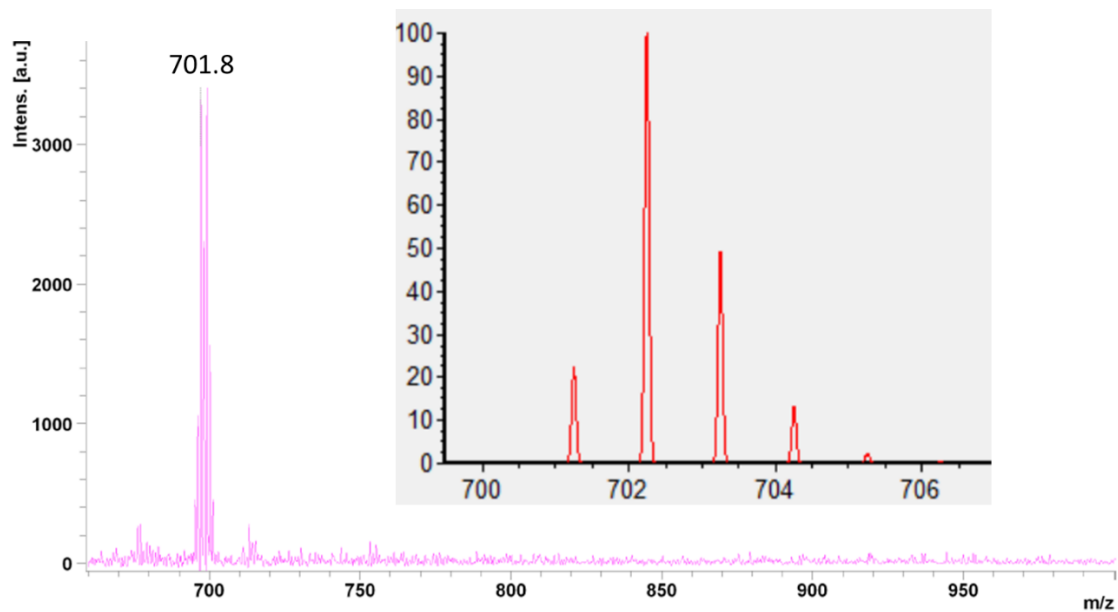


Figure 4.1. Mass spectra of **POR(H₂)**.

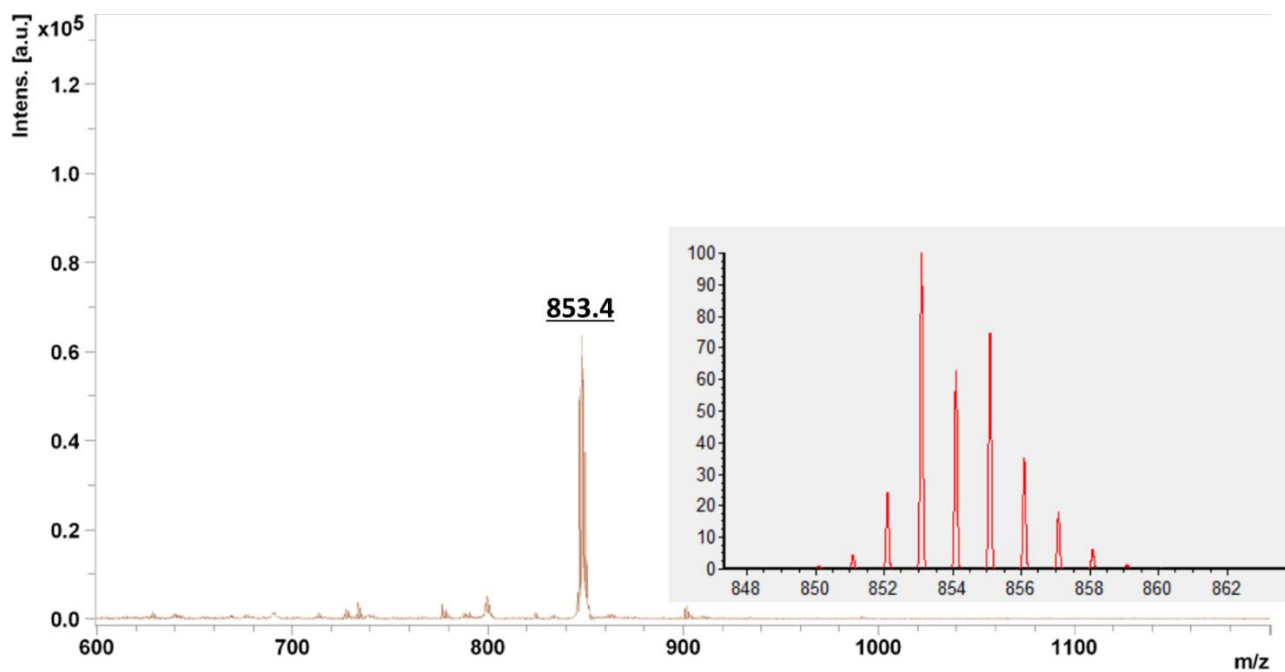


Figure 4.2. Mass spectra of **POR(In)**.

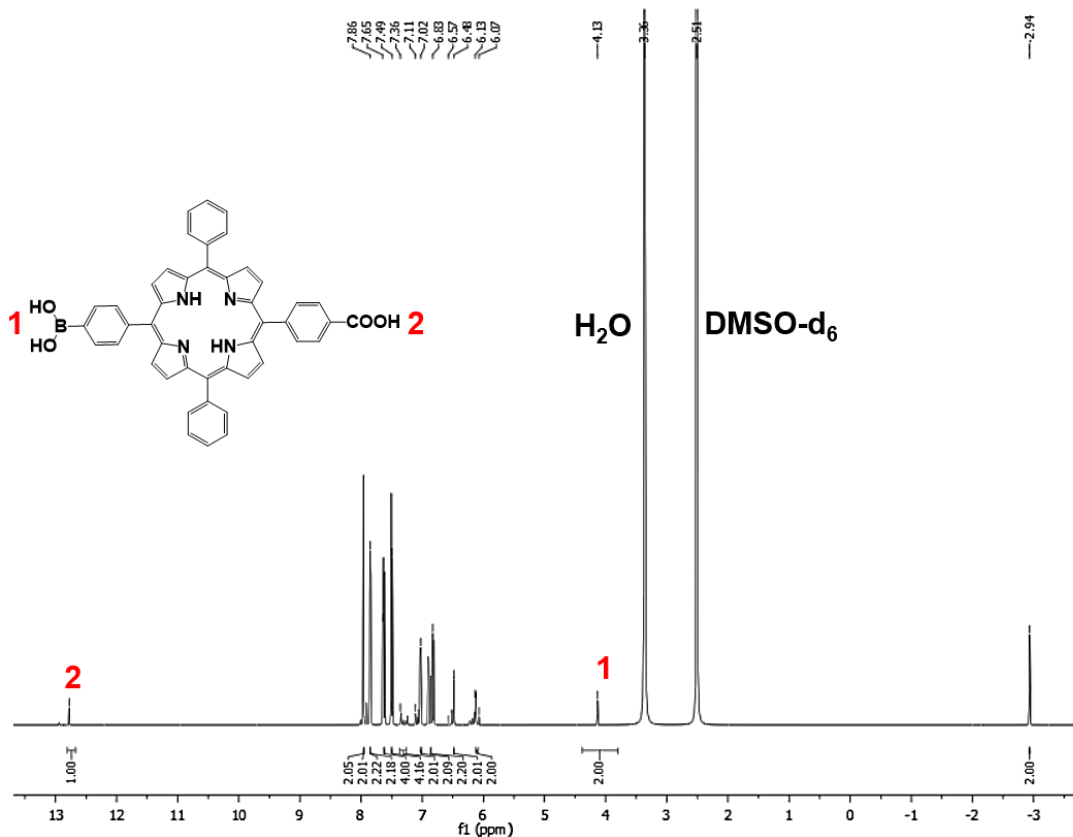


Figure 4.3. ¹H-NMR spectrum of POR(H₂).

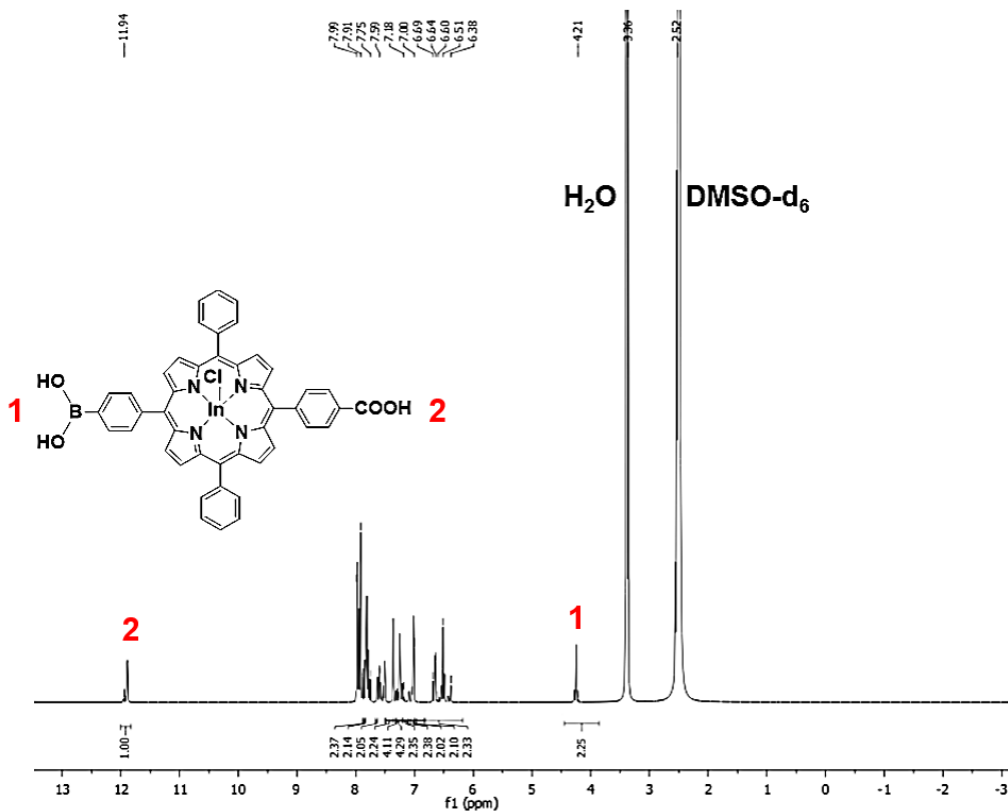


Figure 4.4. ¹H-NMR spectrum of POR(In).

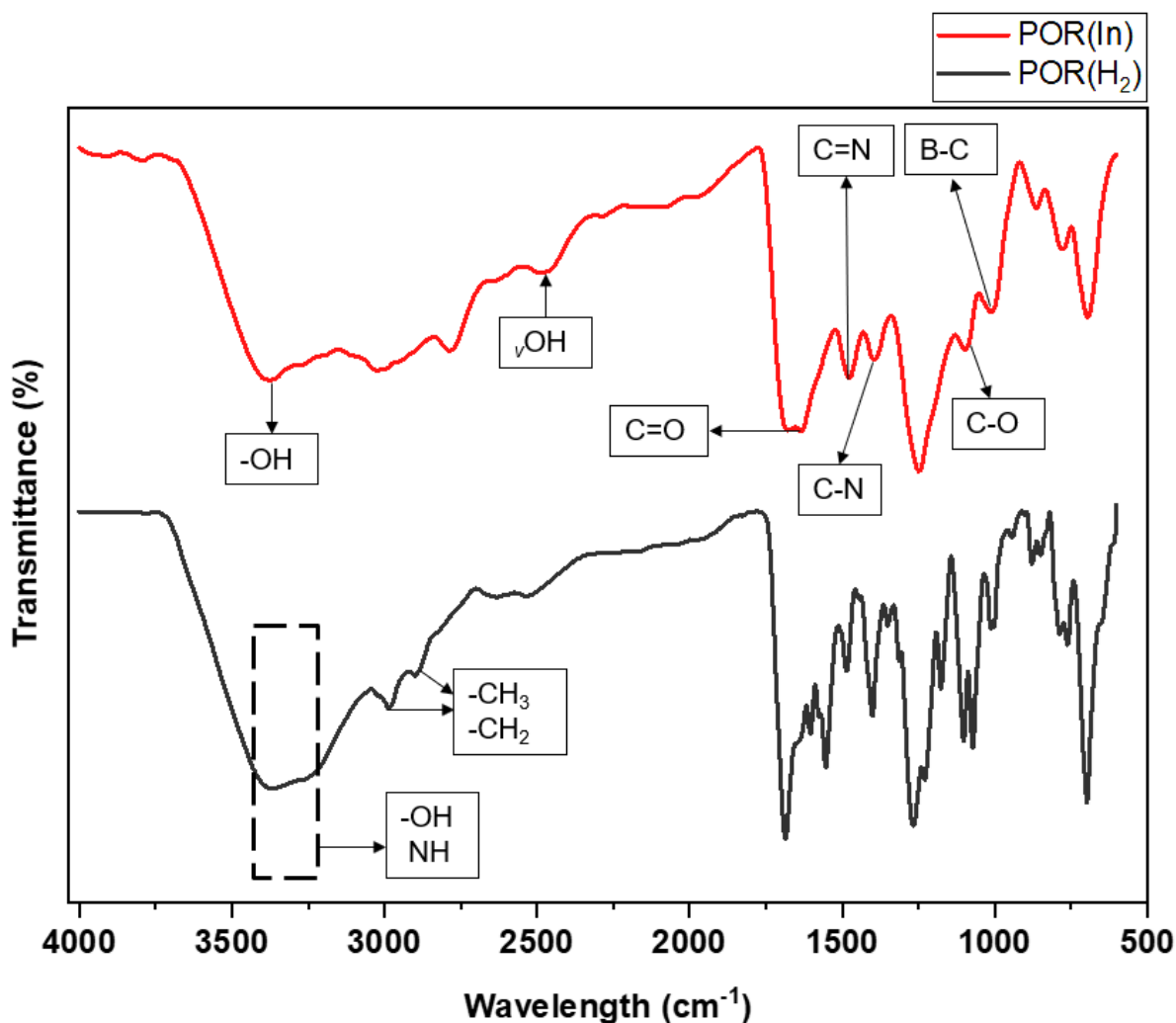


Figure 4.5. FTIR spectra of **POR(H₂)** and **POR(In)**.

4.2.2 UV/Vis spectroscopy

Porphyrins are characterized by pronounced UV/Vis absorption in the visible and ultraviolet range. This is represented by a weak Q band and a strong Soret band, as shown in **Figure 4.6**. Due to the highly conjugated pi-electron system, a strong colour of the porphyrins is observed in solution or solid phase. Soret bands of POR(H₂) and POR(In) were observed at 415 nm and 420 nm, respectively, when dissolved in DMSO. The introduction of indium causes a red shift and delocalization of the porphyrin macrocycle electrons (Giovannetti, 2012), hence the observation in the Soret band of POR(In) as compared to POR(H₂). POR(H₂) and POR(In) are asymmetric porphyrins with boron on one side of the molecule, from which intramolecular energy transfer occurs away from. As a result, porphyrins also exhibit absorption properties like boron dipyrromethene (BODIPY). Typical BODIPY

absorption occurs between 500-518 nm, while porphyrin absorption occurs around 601-649 nm (Jeong et al., 2010). POR(H₂) has absorption bands at 511, 550, 598 and 650 nm, while POR(In) has absorption bands at 517, 554, 599, 598 and 651 nm all of which depicting the Q bands.

Photostability of PS is an important aspect that is closely studied to monitor the photodegradation profile under light irradiation. Photodegradation is an undesirable phenomenon that negatively impacts optimal PS performance. PS with low HOMO energies often exhibit high photostability. This limits the occurrence of photo-oxidation and photo-transformation processes. The chlorinated PS is characterized by a lower HOMO energy and is therefore expected to be more photostable (Sulek et al., 2020). **Figure 4.7** shows the photostability of POR(H₂) and POR(In). POR(In) is the more photostable derivative since the presence of InCl₃ promotes electron-withdrawing effects, promoting reduction and limiting oxidation (Costa et al., 2012).

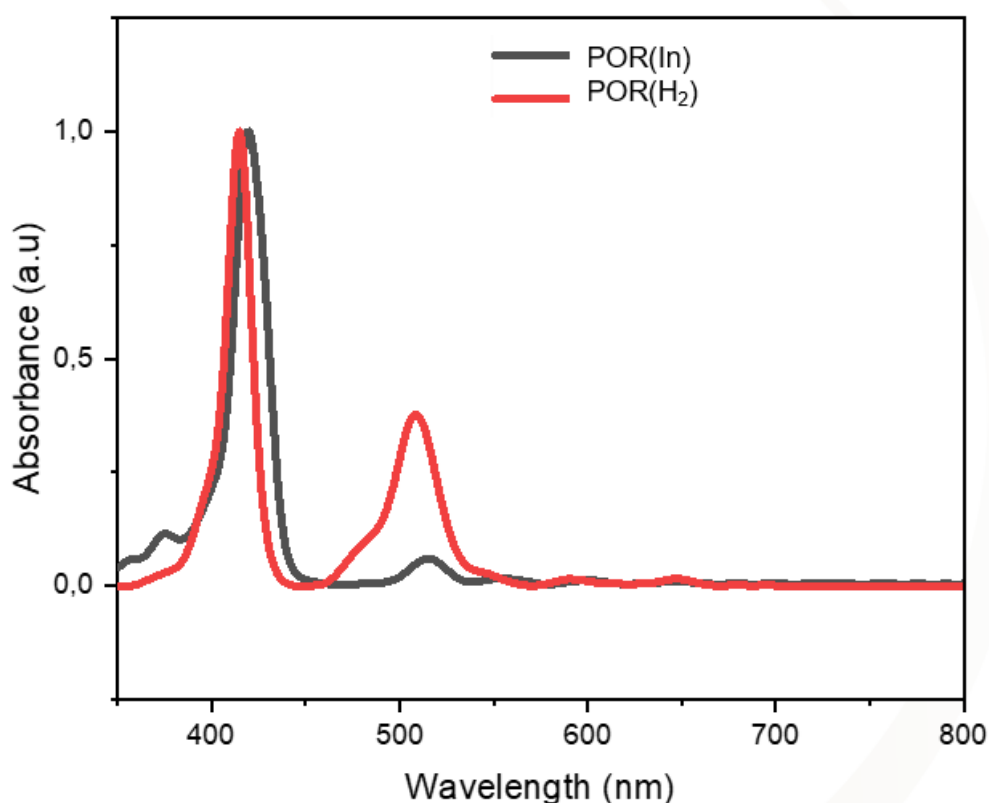


Figure 4.6. Absorption spectra of **POR(H₂)** and **POR(In)** porphyrin derivatives in DMSO.

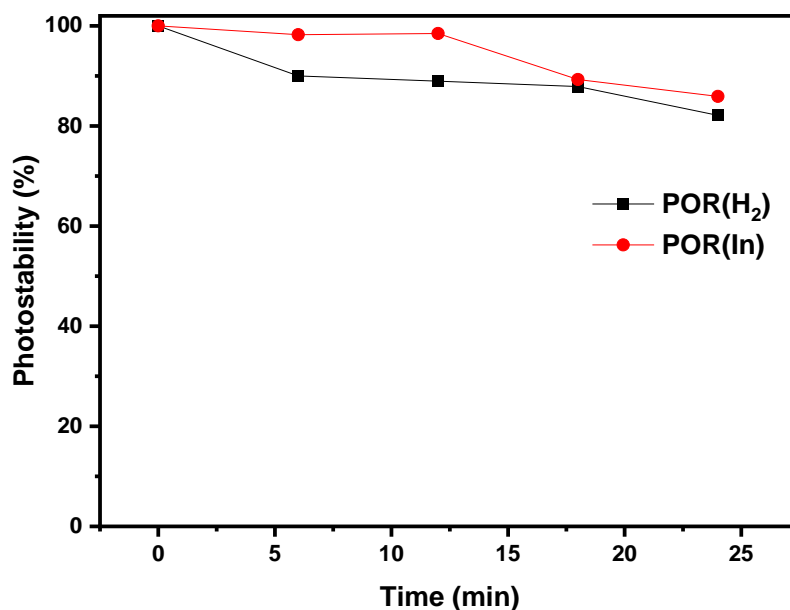


Figure 4.7. The photostability of **POR(H₂)** and **POR(In)** in 2% DMSO.

A red-shift is also observed in the UV/Vis spectroscopy data of the nanoconjugates (**Table 4.1**). **Figure 4.8** shows the absorption spectra of POR(H₂)-CIS/ZnS QD-silica and POR(In)-CIS/ZnS QD-silica, showing absorption bands characteristic of the components forming the complex. Absorption peaks observed at 339 nm, 665 nm, and near-infrared (NIR) represent QD absorption bands. The absorption bands of porphyrins are observed between 400 and 650 nm and are composed of Soret and Q bands. Porphyrin self-assembly was also monitored using UV/Vis spectroscopy. A blue shift in the Soret band absorption with increasing concentration causes the H aggregation, while the redshift induces J aggregation (Ding et al., 2021). **Figure 4.9** shows the UV/Vis spectra of POR(H₂) and POR(In) at increasing concentrations to infer aggregation behaviour. The absorption peaks of both porphyrins did not show any changes in wavelength. This means that POR(H₂) and POR(In) do not aggregate to DMSO at these monitored concentrations.

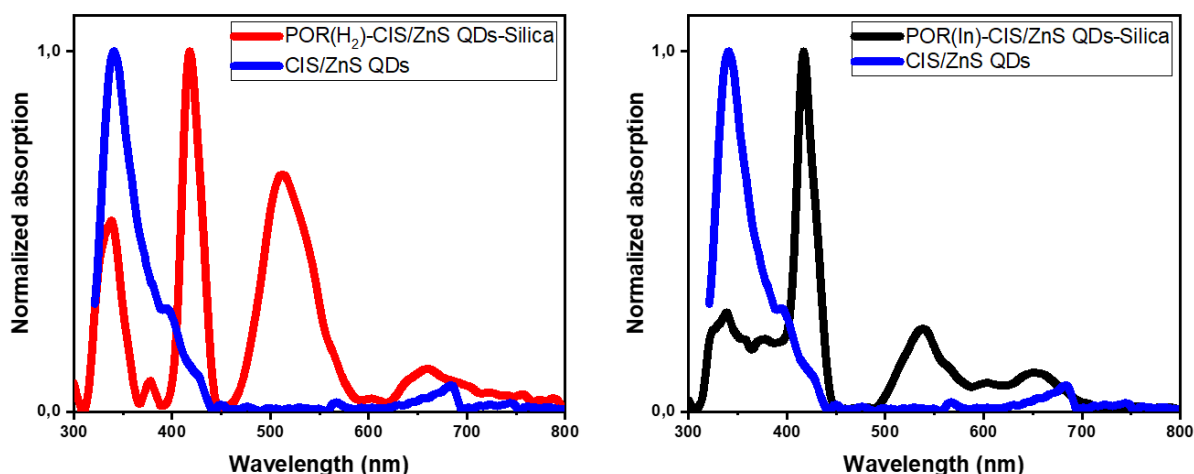


Figure 4.8. Absorption spectra of **POR(H₂)-CIS/ZnS QDs-Silica** and **POR(In)-CIS/ZnS QDs-Silica** compared to **CIS/ZnS QDs** in solid state.

Table 4.1. The photophysical and photochemical parameters for **POR(H₂)**, **POR(In)**, **POR(H₂)-CIS/ZnS QDs-Silica** and **POR(In)-CIS/ZnS QDs-Silica** in DMSO.

Compounds	Soret λ (nm)	τ_F (ns)	Φ_F	τ_T (μ s)	Φ_Δ (± 0.01)
POR(H ₂)	415	7.22	0.043	87.9	0.43
POR(In)	420	5.67	0.025	68.2	0.56
POR(H ₂)-CIS/ZnS QDs-Silica	417	8.67	0.049	40.6	0.59
POR(In)-CIS/ZnS QDs-Silica	421	6.13	0.030	29.7	0.72

$$\Phi_F = \frac{\text{Number of photons emitted}}{\text{Number of photons absorbed}} \dots \dots \dots (\text{e.q. 4.1})$$

$$\Phi_F = \Phi_F^{\text{std}} \times \frac{F A^{\text{std}} n^2}{F^{\text{std}} A (n^{\text{std}})^2} \dots \dots \dots (\text{e.q. 4.2})$$

Where Φ_F^{std} is the fluorescence quantum yield of the standard, F and F^{std} are the areas under the fluorescence curve for sample and standard, respectively. A and A^{std}

are the absorbance of the sample and standard, respectively. n and n^{std} are the refractive indices of the solvent used for sample and standard, respectively.

$$\Phi_{\Delta} = \Phi_{\text{F}}^{\text{std}} \times \frac{B I^{\text{std}}}{B^{\text{std}} I} \dots\dots\dots (\text{e.q. 4.3})$$

Where B and B^{std} are photobleaching rates of the singlet oxygen quencher in the presence of porphyrin derivatives under investigation and the standard, respectively. I and I^{std} are the rates of light absorption by the sample and standard, respectively.

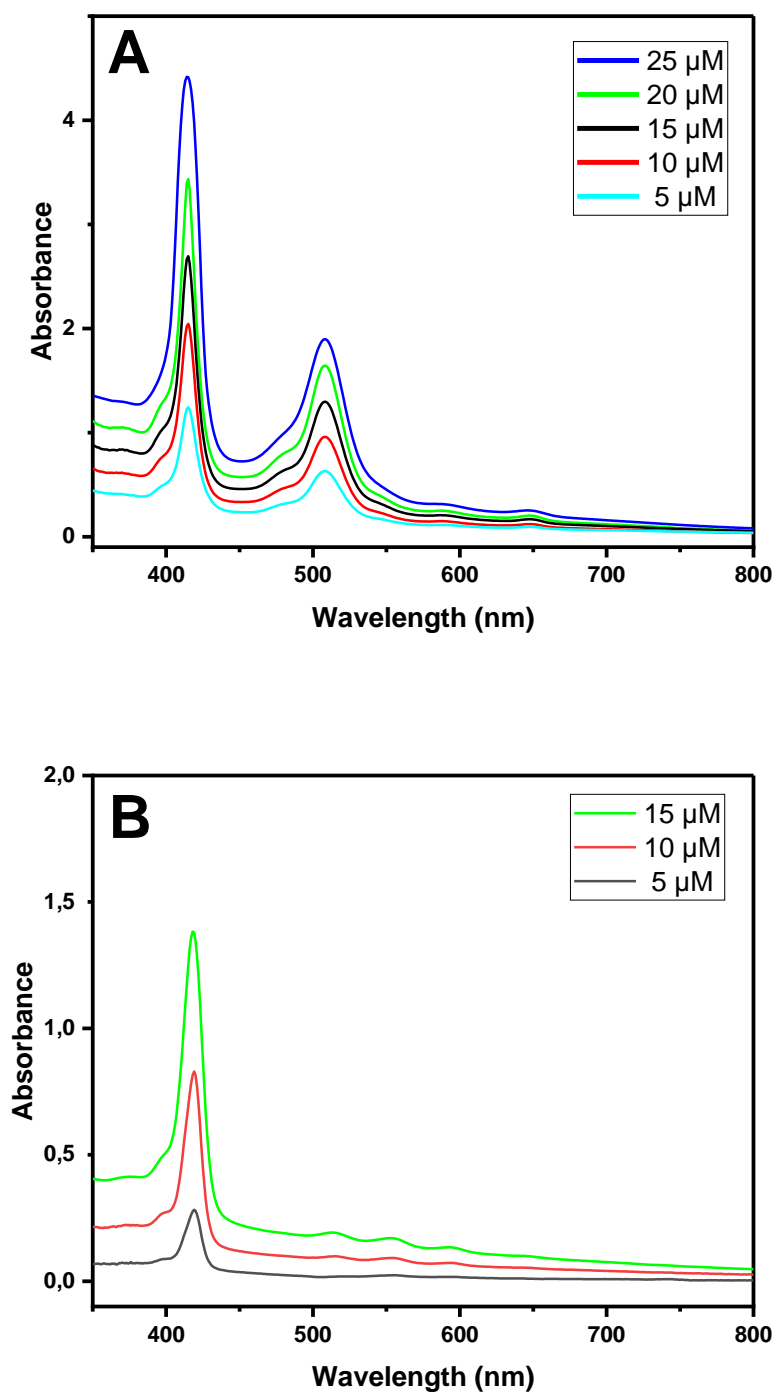


Figure 4.9. Aggregation behaviour of **(A) POR(H₂)** and **(B) POR(In)** in DMSO at different concentrations.

4.2.3 Fluorescence emission spectra

Porphyrins were dissolved in DMSO, and fluorescence emission spectra were recorded. Upon excitation at 405 and 410 nm, the emission peaks for POR(H₂) were

observed at 655 and 720 nm due to Q00 and Q01 transitions, respectively (Soy et al., 2019). Emission peaks of POR(In) were observed at 609 and 660 nm (**Figure 4.10**). The difference between POR(H₂) and POR(In) is a result of metalation, due to a transfer of energy from the lowest excited singlet state to another electronic state of the metal.

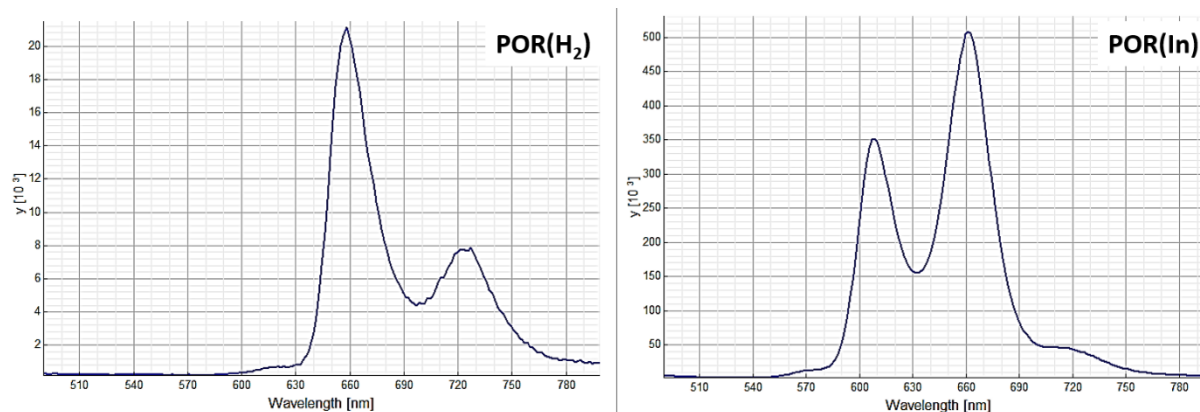


Figure 4.10. Fluorescence emission spectra of **POR(H₂)** and **POR(In)** as examples, excited at $\lambda = 405$ and 410 nm, respectively.

4.2.4 Dynamic light scattering (DLS)

The average size distribution of the nanocomposites was determined using DLS measurements (**Figure 4.11**). The CIS/ZnS-QDs-silica complexes are smaller in size compared to their complexes with porphyrins. Moreover, the POR(H₂)-CIS/ZnS-QDs-silica composites are small compared to the corresponding metalated composites. The size is affected by the change in hydrophobicity induced by the central metal within the porphyrin cavity. Therefore, larger sizes are observed for POR(In)-CIS/ZnS-QDs-silica composites. Sizes of 195, 223, and 256 nm were determined for CIS/ZnS QD silica, POR(H₂)-CIS/ZnS QD silica, and POR(In)-CIS/ZnS QD silica, respectively. The increase in size is evidence of peptide and ester bond formation between the porphyrin, quantum dots and silica.

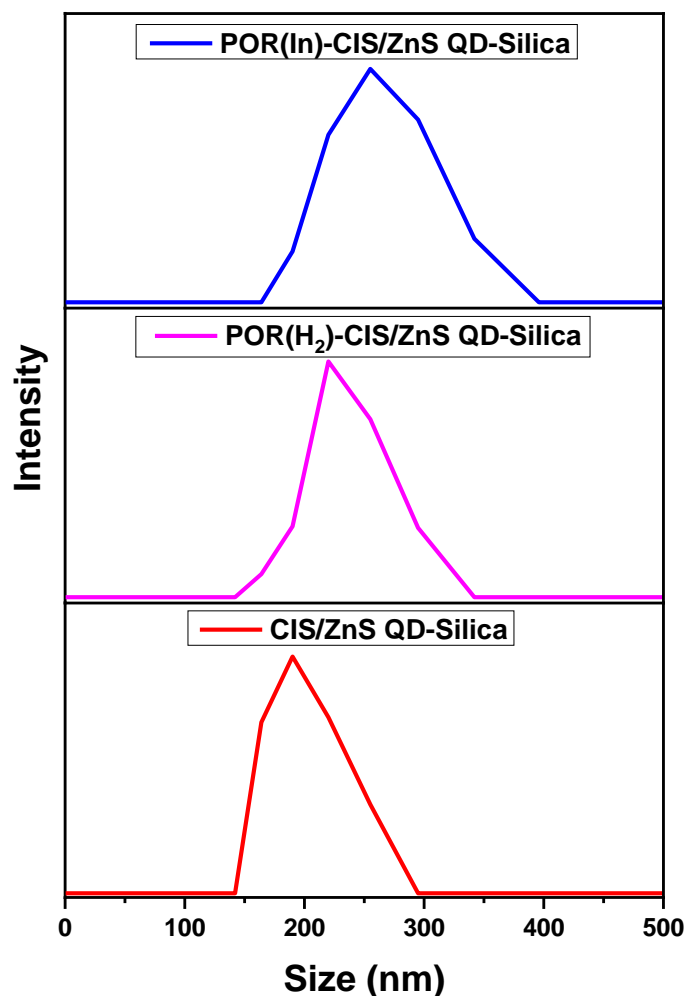


Figure 4.11. Dynamic light scattering (DLS) distribution curve for **CIS/ZnS QDs-Silica**, **POR(H₂)-CIS/ZnS QDs-Silica** and **POR(In)-CIS/ZnS QDs-Silica** in 2% DMSO.

4.2.5 X-ray diffraction (XRD)

The powder X-ray diffraction patterns of both nanocomposites show polycrystalline and single-phase character, as shown in **Figure 4.12**. However, this XRD pattern of mesoporous silica (**Figure 4.13**) shows an amorphous nature. Therefore, this can be attributed to the crystallinity and conjugation of porphyrins and quantum dots on the mesoporous silica surface.

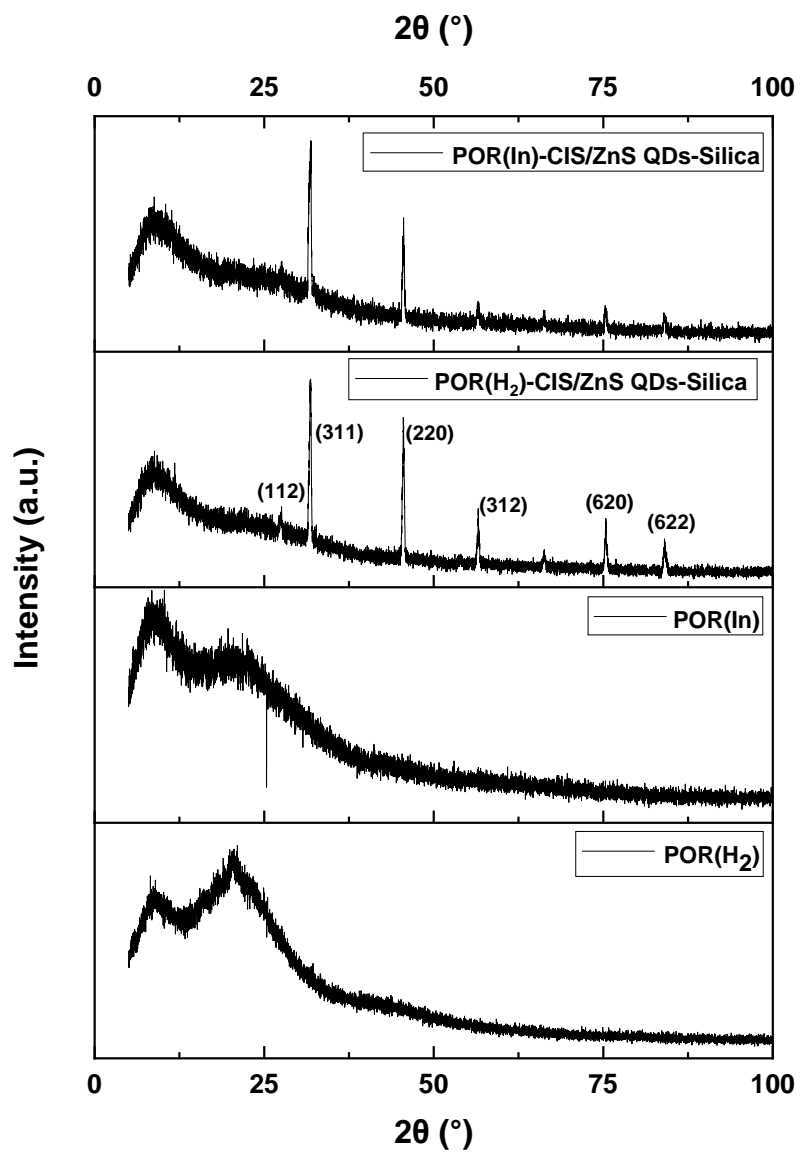


Figure 4.12. XRD patterns of POR(H₂), POR(In), POR(H₂)-CIS/ZnS QDs-Silica and POR(In)-CIS/ZnS QDs-Silica.

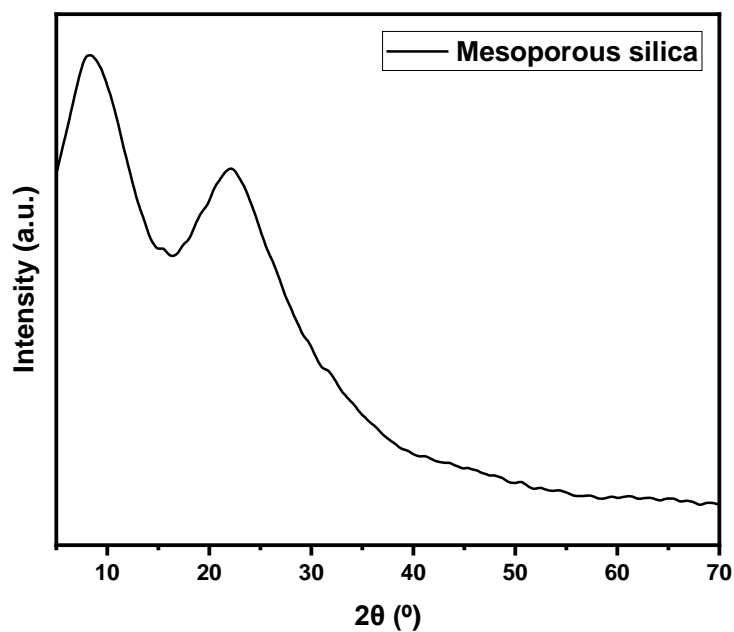


Figure 4.13. XRD pattern of mesoporous silica.

4.2.5 Thermogravimetric analysis (TGA)

TGA revealed the excellent thermal stability of mesoporous silica while acting as a nanocarrier. The conjugated complexes show an improved percentage mass loss to 10% at 800 °C compared to a 50% mass loss of unconjugated POR(H₂) and POR(In) at the same temperature (**Figure 4.14**). The findings also suggest a better thermal stability of POR(H₂)-CIS/ZnS QDs-Silica and POR(In)-CIS/ZnS QDs-Silica.

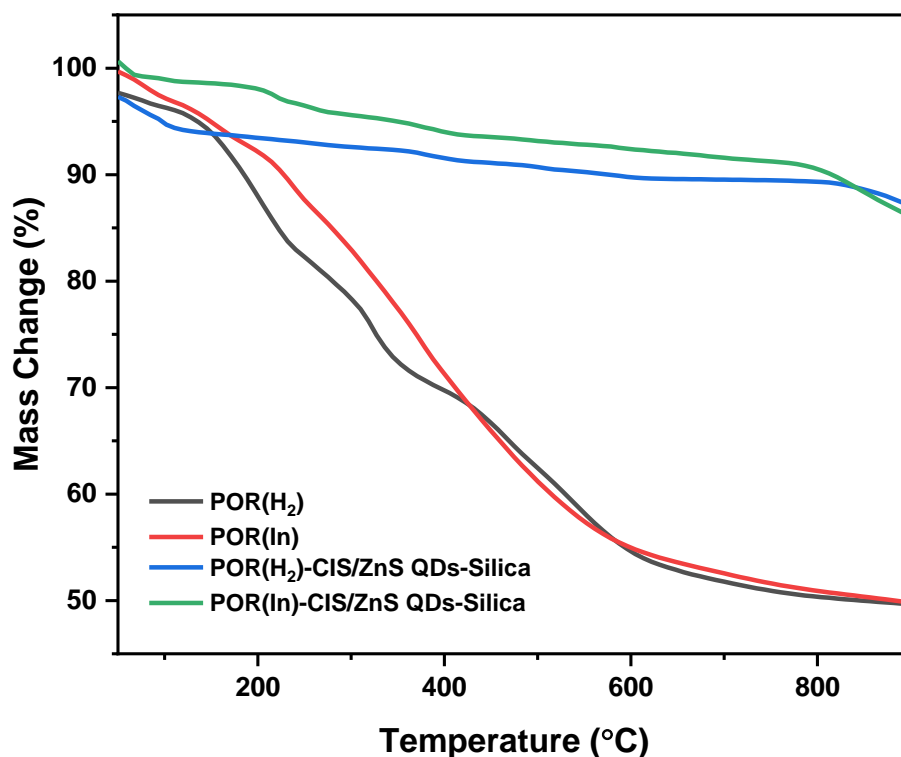


Figure 4.14. Thermogravimetric analysis of **POR(H₂)**, **POR(In)**, **POR(H₂)-CIS/ZnS QDs-Silica** and **POR(In)-CIS/ZnS QDs-Silica**.

4.2.6 N₂ sorption studies

The nature of the porous nanoconjugates was examined via N₂ adsorption-desorption analysis. Findings correspond to type IV isotherms by the International Union of Pure and Applied Chemistry (IUPAC) classification (Donohue and Aranovich, 1998). Which classifies the mesoporous nanomaterial sizes between 2-50 nm (Madima et al., 2022). The isotherms of **POR(H₂)-CIS/ZnS QDs-Silica** and **POR(In)-CIS/ZnS QDs-Silica** possess an H3-type hysteresis loop suggesting a slit-like pore structure as shown in **Figure 4.15** (Thommes et al., 2015).

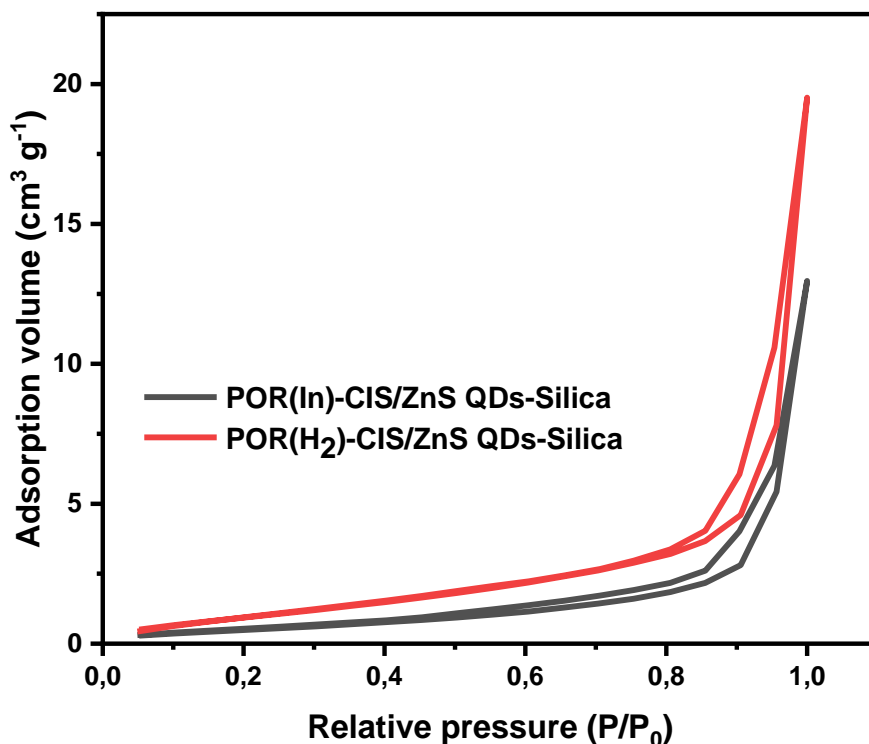


Figure 4.15. N₂ adsorption or desorption isotherms at 77K.

4.2.7 Scanning electron microscopy (SEM)

The morphology and particle distribution of the nanoconjugates were studied using SEM images. **Figure 4.16 and 4.17** shows bulky mesoporous silica with amorphous nature covered with porphyrin-supported spherical quantum dots on the surface of mesoporous silica. On the other hand, **Figure 4.18** shows only mesoporous silica with prominent porosity veins. In **Figure 4.16 and 4.17**, it is observed that the CIS/ZnS QDs adhere to the mesoporous silica surface and act as nanocarriers. Overall, both nanocomposites exhibited identical morphological properties using SEM.

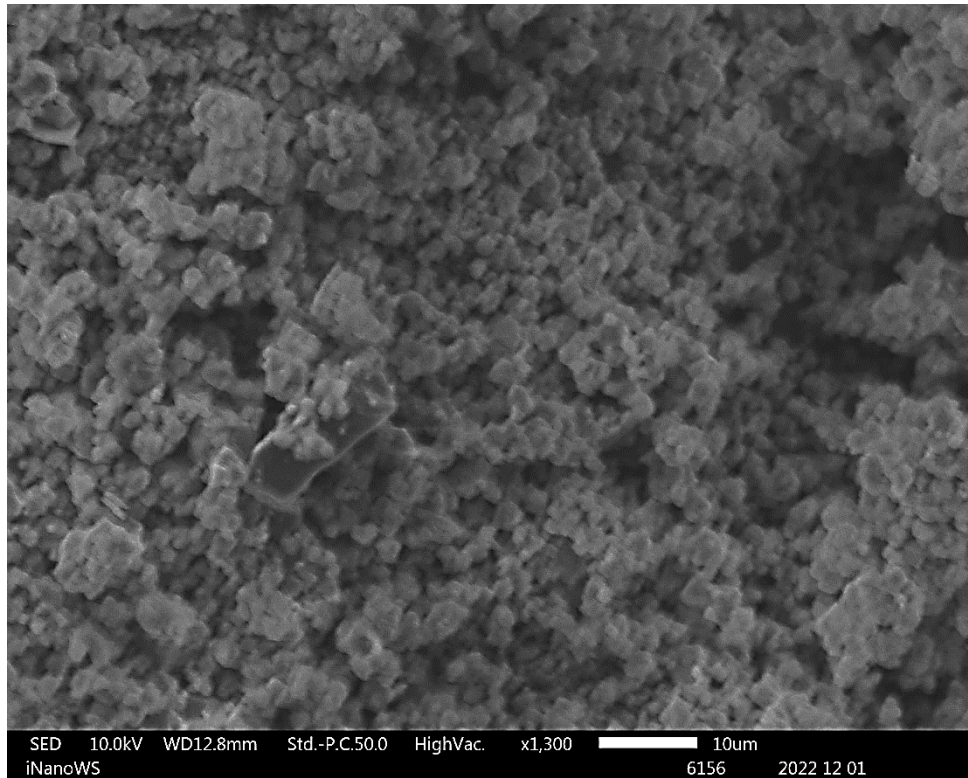


Figure 4.16. SEM image of **POR(H₂)-CIS/ZnS QDs-Silica.**

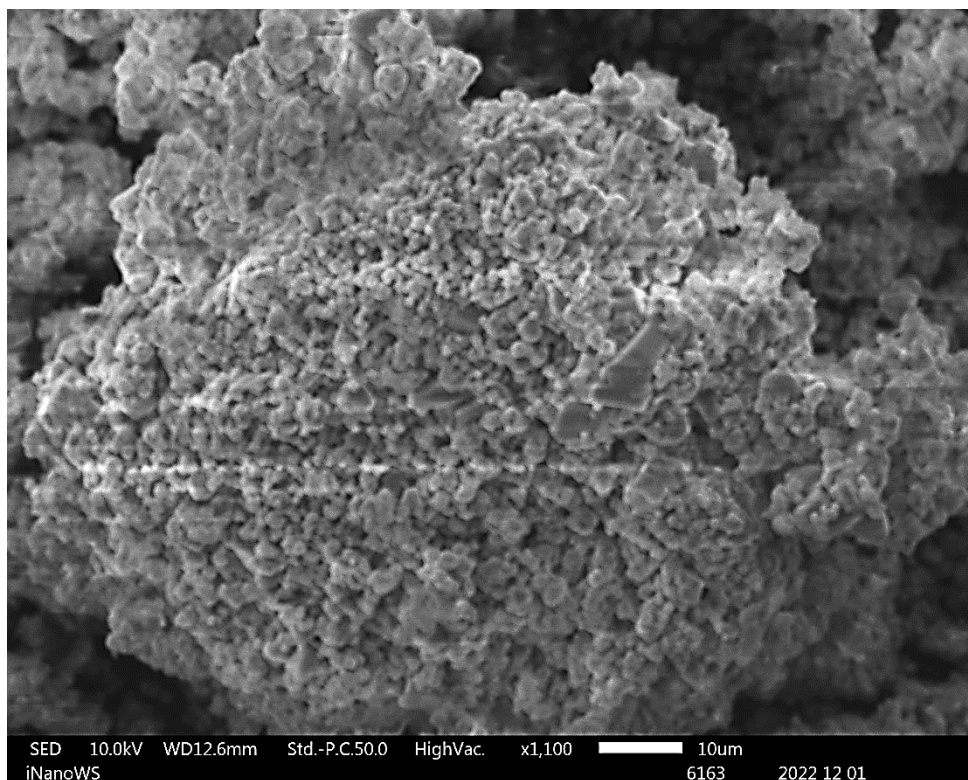


Figure 4.17. SEM image of **POR(In)-CIS/ZnS QDs-Silica.**

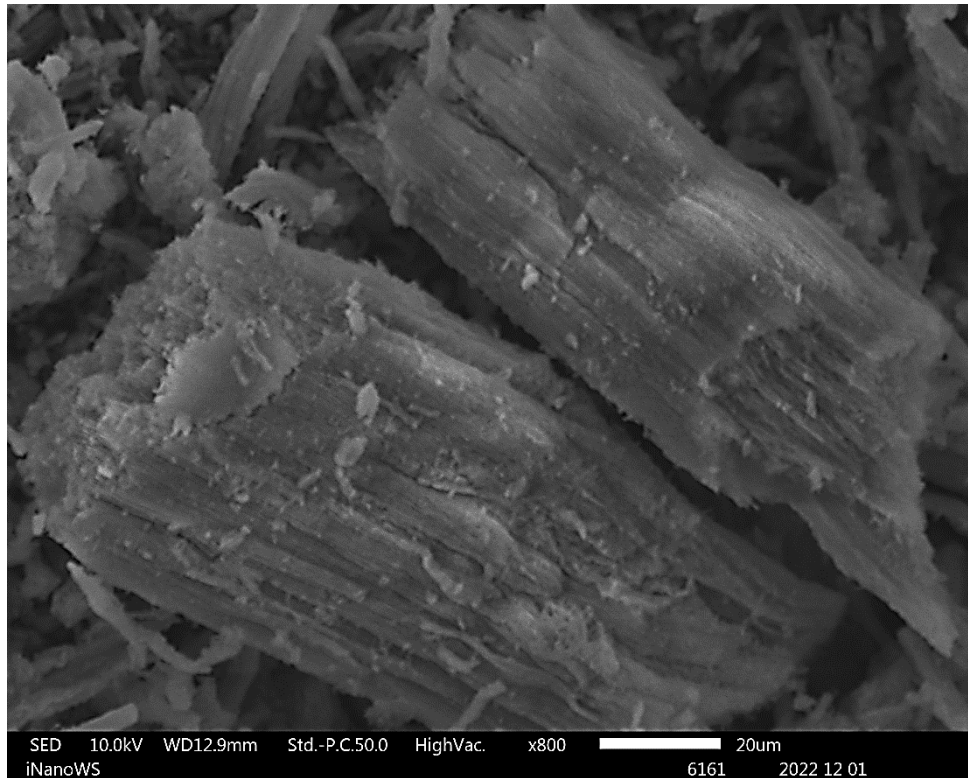


Figure 4.18. SEM image of mesoporous silica.

4.2.7 Energy dispersive microscopy (EDS)

Energy dispersive microscopy (EDS) was used for qualitative analysis of the elemental composition of the synthesized nanocomposites. The elemental compositions of POR(H₂)-CIS/ZnS-QD silica and POR(In)-CIS/ZnS-QD silica are shown in **Figure 4.19**. The synthesized nanocomposite exhibits the expected elements. The Cu, In, S and Zn peaks are related to the composition of the CIS/ZnS QDs. Because the surface of mesoporous silica is covered with QDs, the elemental composition of some materials could only be vaguely determined. Therefore, the detected elements correspond to CIS/ZnS QDs. Carbon was abundantly present as well, due to organic compounds used in the conjugation and synthesis process.

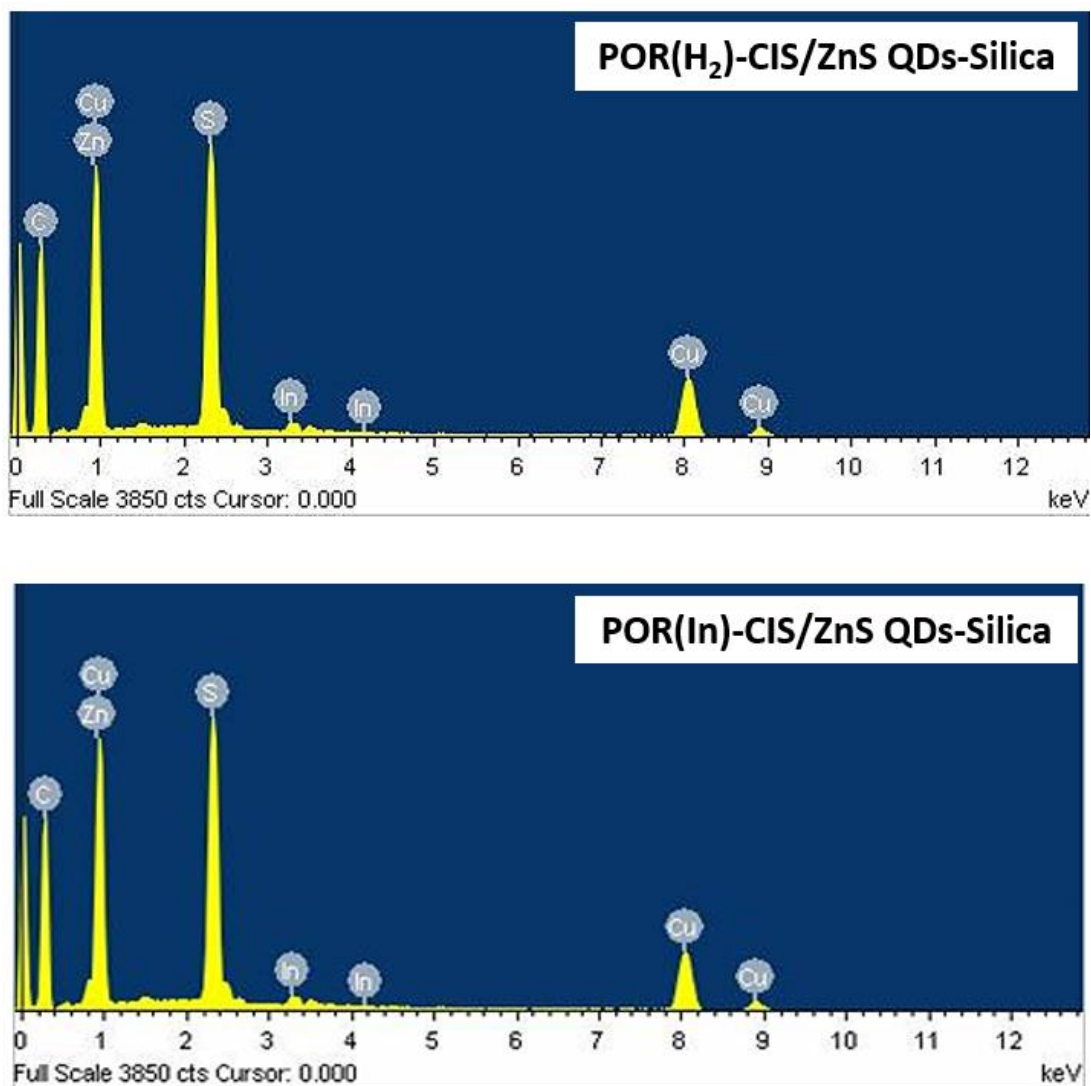


Figure 4.19. EDS images of **POR(H₂)-CIS/ZnS QDs-Silica** and **POR(In)-CIS/ZnS QDs-Silica**.

4.2.8 Fluorescence lifetimes (τ_F) and quantum yield (Φ_F)

Fluorescence lifetime (τ_F) is the average time a fluorophore spends in the singlet excited state before emitting a photon and returning to the ground state (Matarazzo and Hudson, 2015). Fluorescence decay curves and τ_F analysis were recorded using time-correlated single photon counting (TCSPC). **Figure 4.20** shows the fluorescence decay curve of POR(In)-CIS/ZnS QD silica as an example. For POR(H₂), POR(In), POR(H₂)-CIS/ZnS QDs-silica, and POR(In)-CIS/ZnS QDs-silica, τ_F is 7.22, 5.67, 8.67, and 6.13 ns, respectively (**Table 4.1**).

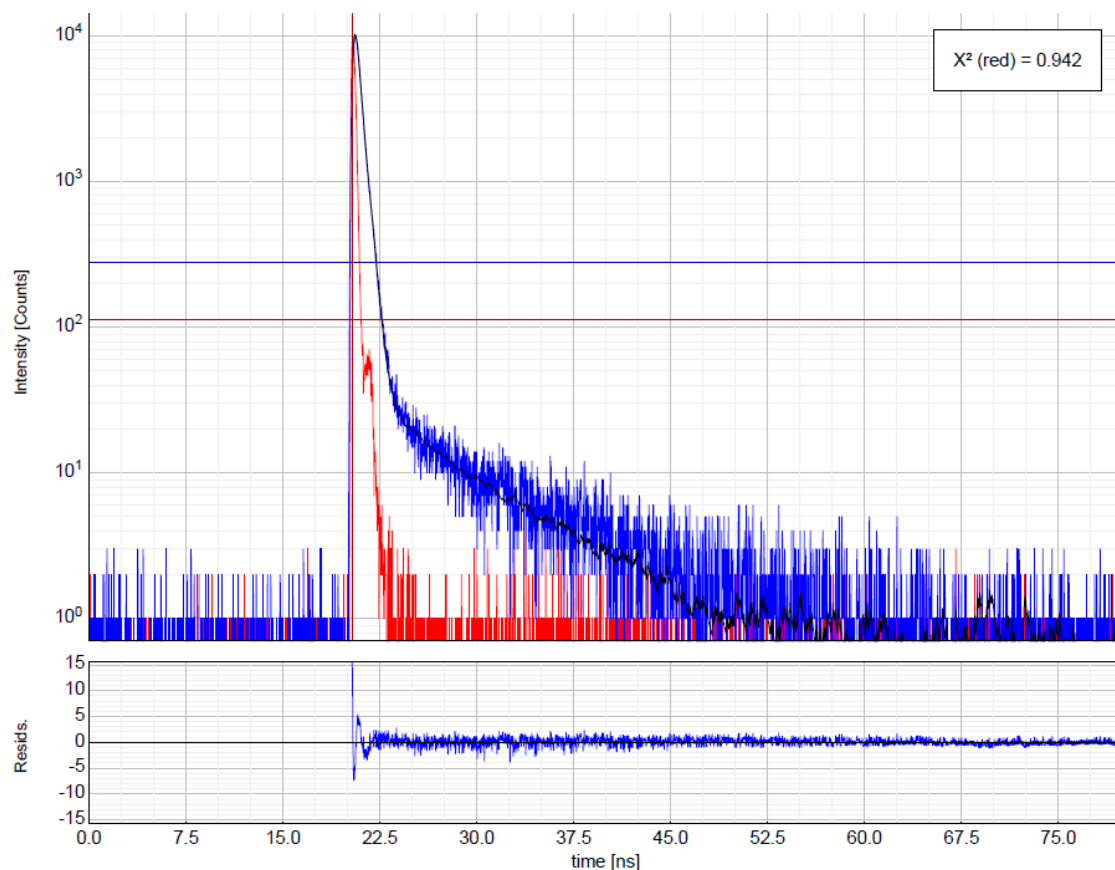


Figure 4.20. Fluorescence decay (blue), X^2 fitting (black) and IRF (red) curves for **POR(In)-CIS/ZnS QDs-Silica** in DMSO.

The fluorescence quantum yield (Φ_F) value indicates the ratio of emitted photons to those initially absorbed by fluorescence. They show how an excited molecule efficiently returns to the electronic ground state upon photon emission. This process is influenced by various parameters such as electronic structure, steric and conformational interactions (Lakowicz, 2006). Φ_F values were obtained using methods reported in the literature, with $\Phi_F=0.039$ for ZnTPP (TPP=tetraphenylporphyrin) as a standard (Brookfield et al., 1986; MacRobert et al., 1989; Ogunsipe et al., 2004). Calculations show that the Φ_F values of the non-metalated derivatives are higher than those of the corresponding metalated derivatives. Metalation was the main principle of this observation, as it facilitates fluorescence quenching (Hayashi et al., 2014). Φ_F values were determined as 0.043, 0.025, 0.049 and 0.030 for POR(H_2), POR(In), POR(H_2)-CIS/ZnS QDs-silica, and POR(In)-CIS/ZnS QDs-silica, respectively (**Table 4.1**).

4.2.9 Singlet oxygen quantum yield (Φ_{Δ})

Generation of singlet oxygen is a key component of porphyrin efficacy in photoinactivation of microorganisms by oxidative stress (DeRosa, 2002). Φ_{Δ} was analyzed in dry DMF using DMA and ZnTPP (used as standard singlet oxygen quantum yield ($\Phi_{\Delta}^{\text{std}} = 0.53$)) as singlet oxygen quenchers (Kee et al., 2008). Metalated porphyrins are well documented to be more efficient ROS generators compared to their metal-free analogues (Dąbrowski et al., 2015; Skwor et al., 2016). Higher Φ_{Δ} values are reported for POR(In) compared to POR(H₂). Which are also observed this study. The Φ_{Δ} values for POR(H₂) and POR(In) were found to be 0.43 and 0.56, respectively. After bonding, the Φ_{Δ} values of POR(H₂)-CIS/ZnS QDs silica and POR(In)-CIS/ZnS QDs silica were measured to be 0.59 and 0.72, respectively. Notably, the conjugation of porphyrins and quantum dots enhanced the production of singlet oxygen.

As shown in **Figure 4.21**, the Soret and Q bands of POR(H₂) were unchanged during DMA degradation, confirming the photostability of the porphyrin. A similar result is observed for POR(In), as shown in **Figure 4.22**.

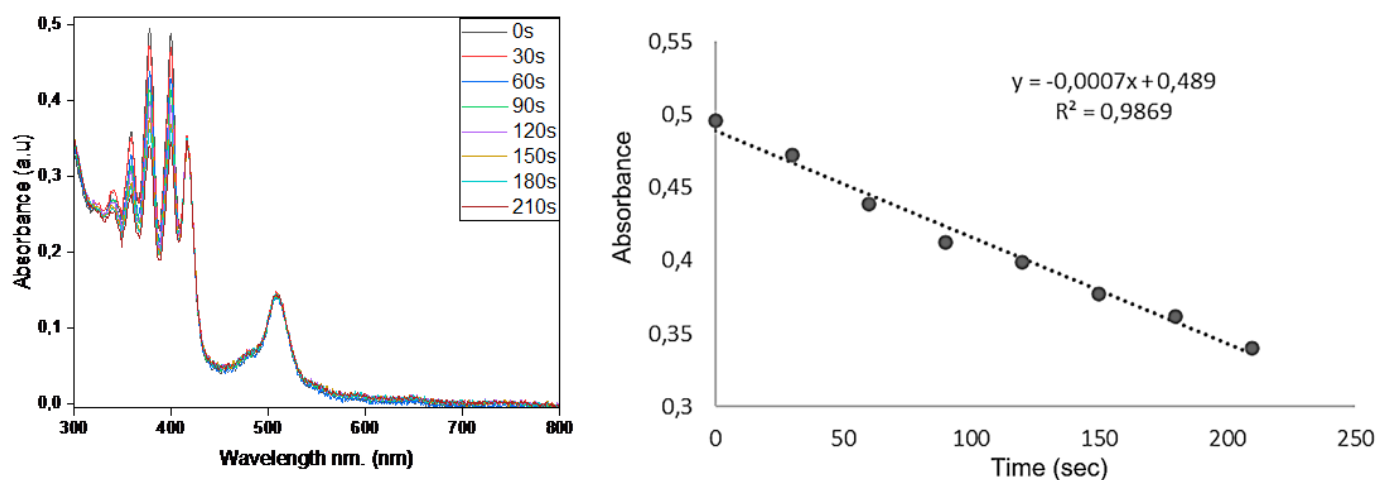


Figure 4.21. Variations in DMA absorption spectra with irradiation time in the presence of **POR(H₂)**.

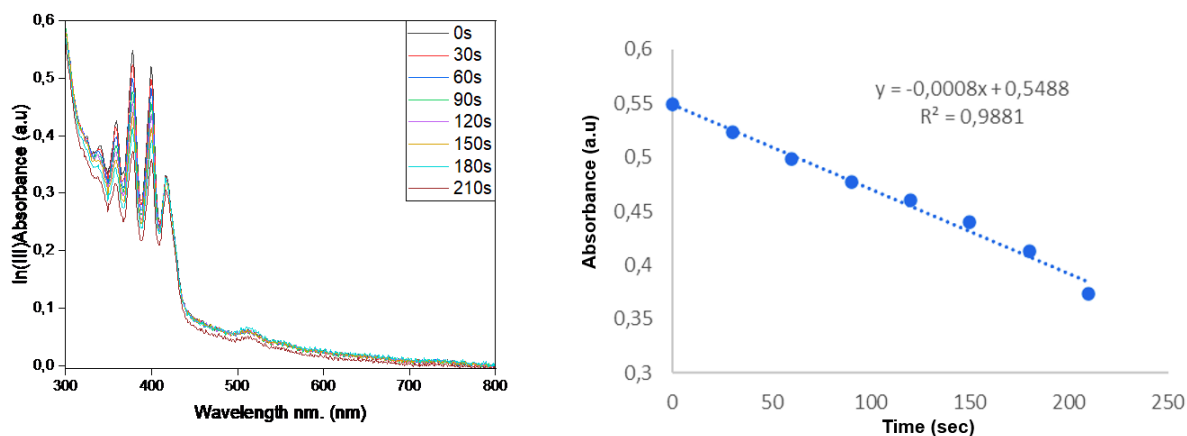


Figure 4.22. Variations in DMA absorption spectra with irradiation time in the presence of **POR(In)**.

4.2.10 Triplet lifetime (τ_T)

To accurately determine the triplet state parameter of the complex, the sample is deoxygenated to prevent oxygen quenching of the triplet state macrocycle (Openda et al., 2022). The sample was degassed with argon for 1 h before recording the triplet lifetime decay curve. The τ_T values obtained are 87.9, 68.2, 40.6, and 29.7 μs for $\text{POR}(\text{H}_2)$, $\text{POR}(\text{In})$, $\text{POR}(\text{H}_2)\text{-CIS/ZnS QDs-silica}$, and $\text{POR}(\text{In})\text{-CIS/ZnS QDs-silica}$ (**Figure 4.23**), respectively. The longest τ_T value determined was for the metal-free derivative, whereas the indium derivative showed a shorter time due to heavy atom effects.

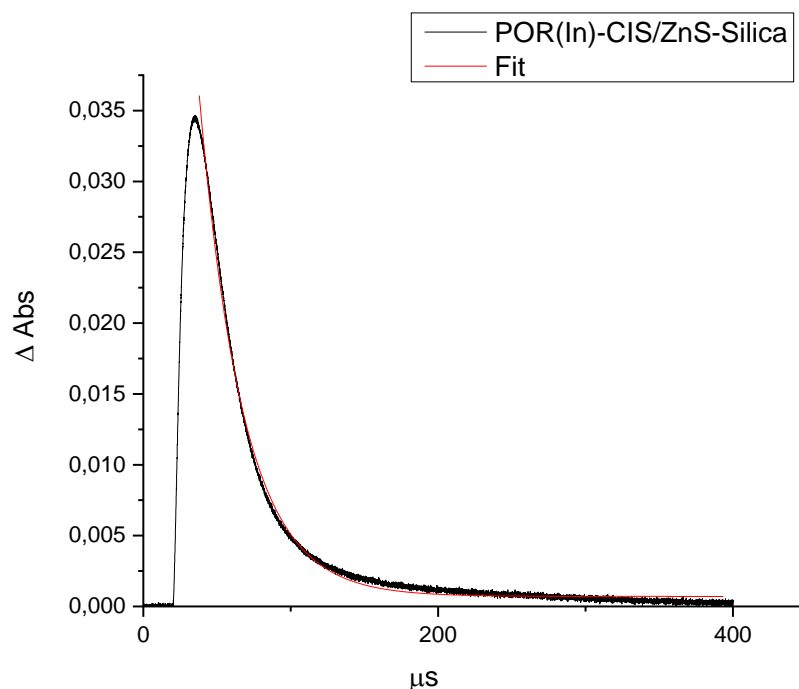


Figure 4.23. Triplet lifetime plot of **POR(In)-CIS/ZnS-Silica** as an example.

4.3 REFERENCES

Brookfield, R.L., Ellul, H., Harriman, A., Porter, G., 1986. *J. Chem. Soc., Faraday Trans. 82*, 219–233.

Costa, D.C.S., Gomes, M.C., Faustino, M.A.F., Neves, M.G.P.M.S., Cunha, Â., Cavaleiro, J.A.S., Almeida, A., Tomé, J.P.C., 2012. *Photochem. Photobiol. Sci.* 11, 1905–1913.

Dąbrowski, J.M., Pucelik, B., Pereira, M.M., Arnaut, L.G., Stochel, G., 2015. *J. Coord. Chem.* 68, 3116–3134.

DeRosa, M., 2002. *Coord. Chem. Rev.* 233–234, 351–371.

Ding, X., Wei, S., Bian, H., Zhu, L., Xia, D., 2021. *Energy & Fuels* 35, 11848–11857.

Donohue, M., Aranovich, G., 1998. *Adv. Colloid Interface Sci.* 76–77, 137–152.

Giovannetti, R., 2012. The Use of Spectrophotometry UV-Vis for the Study of Porphyrins, in: *Macro To Nano Spectroscopy. InTech.4*, 11-16.

Hayashi, K., Nakamura, M., Miki, H., Ozaki, S., Abe, M., Matsumoto, T., Kori, T., Ishimura, K., 2014. *Adv. Funct. Mater.* 24, 503–513.

Jeong, E.-Y., Burri, A., Lee, S.-Y., Park, S.-E., 2010. *J. Mater. Chem.* 20, 10869.

Kee, H.L., Bhaumik, J., Diers, J.R., Mroz, P., Hamblin, M.R., Bocian, D.F., Lindsey, J.S., Holten, D., 2008. *J. Photochem. Photobiol. A Chem.* 200, 346–355.

Lakowicz, J.R. (Ed.), 2006. *Principles of Fluorescence Spectroscopy*. Springer US, Boston, MA. 103, 4357-4366.

MacRobert, A.J., Bown, S.G., Phillips, D., 1989. *Ciba Found. Symp.* 146, 4–16.

Madima, N., Kefeni, K.K., Mishra, S.B., Mishra, A.K., 2022. *Heliyon* 8, 10683.

Ogunsipe, A., Chen, J.-Y., Nyokong, T., 2004. *New J. Chem.* 28, 822–827.

Openda, Y.I., Mgidlana, S., Nyokong, T., 2022. *J. Lumin.* 246, 118863.

Skwor, T.A., Klemm, S., Zhang, H., Schardt, B., Blaszczyk, S., Bork, M.A., 2016. *J. Photochem. Photobiol. B Biol.* 165, 51–57.

Soy, R.C., Babu, B., Oluwole, D.O., Nwaji, N., Oyim, J., Amuhaya, E., Prinsloo, E., Mack, J., Nyokong, T., 2019. *J. Porphyr. Phthalocyanines* 23, 34–45.

Sulek, A., Pucelik, B., Kobielski, M., Barzowska, A., Dąbrowski, J.M., 2020. *Int. J. Mol. Sci.* 21, 8716.

Thommes, M., Kaneko, K., Neimark, A. V., Olivier, J.P., Rodriguez-Reinoso, F., Rouquerol, J., Sing, K.S.W., 2015. *Pure Appl. Chem.* 87, 1051–1069.

CHAPTER 5

ANTIMICROBIAL STUDIES

5.1 INTRODUCTION

In this chapter, the findings of conducted antimicrobial studies using the synthesized nanoconjugates and an irradiation source are discussed.

5.2 METAGENOMIC DATA

The presented data is a profile of microbial diversity as sampled from a wastewater influent collected from a wastewater treatment plant (GPS coordinates: 26.311433, 27.930583) located in the province of Gauteng in South Africa. Metagenomic data was received from Inqaba Biotec as per submitted samples. Taxonomical classification was found to be 100% of kingdom bacteria (**Figure 5.1**). The phylum classification, class classification, order classification, family classification and genus classifications are outlined in **Tables 5.1- 5.5** respectively. The data shows the presence of *E. coli* through classification of kingdom bacteria, phylum proteobacteria, class Gammaproteobacteria, order Enterobacterales, family *Enterobacteriaceae* and genus *escherichia*. A similar conclusion was made for *S. aureus* through classification of kingdom bacteria, phylum firmicutes, class Bacilli and order Bacillales. However, family and genus classification for *S. aureus* were not identified, either due to very low concentrations or categorised as 'unknown'. Because colony growth was still established when mannitol salt agar was used for the isolation.

Taxonomical Classification

Kingdom Classification

Kingdom	Read Count	%
Bacteria	13904.0	100.00

Top Kingdom Classification

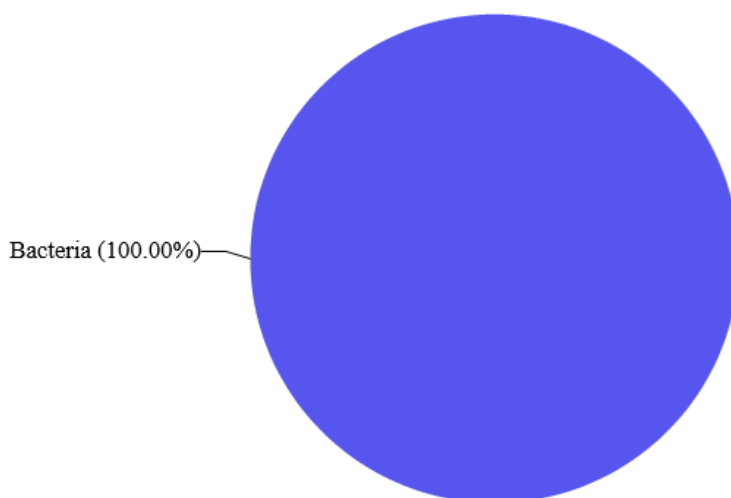


Figure 5.1. Taxonomical classification.

Table 5.1. Phylum Classification.

Phyla Classification	Read Count	%
Proteobacteria	11712.0	84.23
Firmicutes	2061.0	14.82
Unknown	124.0	0.89
Bacteroidota	7.0	0.05

Table 5.2. Class Classification.

Class	Read Count	%
Gammaproteobacteria	11712.0	84.23

Bacilli	2059.0	14.81
Unknown	124.0	0.89
Bacteroidia	7.0	0.05
Clostridia	2.0	0.01

Table 5.3. Order Classification.

Order	Read Count	%
Pseudomonadales	3862.0	27.78
Enterobacterales	3830.0	27.55
Aeromonadales	2111.0	15.18
Bacillales	2023.0	14.55
Unknown	1729.0	12.44
Burkholderiales	174.0	1.25
Vibrionales	75.0	0.54
Alteromonadales	63.0	0.45
Lactobacillales	26.0	0.19
Bacteroidales	7.0	0.05
Christensenellales	2.0	0.01
Xanthomonadales	2.0	0.01

Table 5.4. Family Classification.

Family	Read Count	%
Pseudomonadaceae	3732.0	26.85
Enterobacteriaceae	3413.0	24.55
Unknown	2165.0	15.57
Aeromonadaceae	2111.0	15.18
Bacillaceae	2005.0	14.42
Alcaligenaceae	151.0	1.09
Moraxellaceae	106.0	0.76
Vibrionaceae	75.0	0.54
Shewanellaceae	63.0	0.45

Enterococcaceae	26.0	0.19
Comamonadaceae	18.0	0.13
Morganellaceae	16.0	0.12
Planococcaceae	11.0	0.08
Tannerellaceae	6.0	0.04
Christensenellaceae	2.0	0.01
Xanthomonadaceae	2.0	0.01

Table 5.5. Genus Classification.

Genus	Read Count	%
Unknown	3741.0	26.91
Pseudomonas	3732.0	26.85
Aeromonas	2111.0	15.18
Bacillus	2005.0	14.42
Escherichia	1655.0	11.90
Enterobacter	189.0	1.36
Acinetobacter	100.0	0.72
Kerstersia	93.0	0.67
Vibrio	75.0	0.54
Shewanella	63.0	0.45
Enterococcus	26.0	0.19
Citrobacter	24.0	0.17
Alcaligenes	20.0	0.14
Comamonas	13.0	0.09
Providencia	12.0	0.09
Raoultella	11.0	0.08
Klebsiella	7.0	0.05
Kurthia	6.0	0.04
Macellibacteroides	6.0	0.04
Lysinibacillus	5.0	0.04

Morganella	4.0	0.03
Christensenellaceae_R	2.0	0.01
Buttiauxella	2.0	0.01

5.3 IN VITRO ANTIMICROBIAL STUDIES

The Gram (-) bacterial strain used in this study was *Escherichia coli*, whereas *Staphylococcus aureus* was used to study the Gram (+) bacterial strains. All photoinactivation studies were performed using 2 % DMSO in PBS. Triplicating the photoinactivation procedure for each sample increased the reliability and validity of the results. A concentration of 10 µg/mL of the nanoconjugate was used for photoinactivation studies. Bacteria/nanoconjugate mixture was incubated for 30 min at 37 °C in the dark in a shaker oven prior to plating. 100 µL of solution was taken from the suspension and immediately inoculated onto agar plates to measure 0 min activity without treatment. 2.5 mL of each incubated bacterial/nanoconjugate suspension was then transferred to a 24-well plate for 5-, 10- and 15-min measurements in the presence of light simulation. The number of colonies on each plate was then counted after incubation at 37 °C. Control treatments were performed in the absence of photosensitizer, both with illumination and in the dark, to examine the effects of light and solvent on the bacteria. The CFU/mL data were transformed to logarithmic form and the percentage reduction was calculated.

The Food and Drug Administration (FDA) recommends a minimum 3 log CFU reduction for PS to be considered suitable for photoinactivation (Sobotta et al., 2019). The results of this study suggest that photoinactivation of *E. coli* with POR(H₂) and POR(In) is not recommended since it does not meet the requirements. POR(H₂) and POR(In) against *E. coli* achieved log reductions of 1.47 and 1.49 log CFU, respectively. On the other hand, a CFU reduction of 9.76 log was achieved for *S. aureus* when exposed to both porphyrins and in this case meets FDA recommendations. This suggests that nonionic porphyrins are less potent against Gram(-) bacteria and more potent against Gram(+) bacteria. Gram(-) bacteria have an anionic surface and inhibit electrostatic interactions with nonionic porphyrins (Hamblin,

2016). Further observation showed that porphyrin phototoxicity was directly proportional to irradiation time (**Figures 5.2 and 5.3**).

Nanocomposites of porphyrins and quantum dots enhanced photoinactivation properties compared to their individual analogues, binding results in a synergistic effect induced by the components of the conjugate (Openda et al., 2021). In another study, Magaela et al. shown that conjugation of cationic 5,10,15,20-tetra(pyridine-3-yl)porphyrin and Zn(II) derivatives to graphene quantum dots improves photoinactivation, resulting in high Φ_F and high Φ_{Δ} values (N. B. Magaela et al., 2022). Similarly, this study provided corresponding results when POR(H₂) and POR(In) were bound to CIS/ZnS QDs and mesoporous silica as a support. POR(H₂)-CIS/ZnS QD silica and POR(In)-CIS/ZnS QD silica achieved complete photoinactivation of *S. aureus* with a 8.08 and 9.76 log reduction in CFU respectively. The nanocomposite also produced a comparable log reduction of 9.38 log CFU compared to *E. coli*. Findings show that CIS/ZnS QDs could potentially offset the drawbacks of nonionic porphyrins against Gram(-) bacteria. Overall, details of bacterial viability in the presence of porphyrins and nanoconjugates are shown in **Tables 5.6 and 5.7**. *E. coli* was viable after 15 min of irradiation in the presence of POR(H₂) and POR(In), but no viability was detected when **POR(H₂)-CIS/ZnS QDs-Silica** and **POR(In)-CIS/ZnS QDs-Silica** were utilized. *S. aureus* showed poor viability to porphyrins and nanoconjugates. No viability was observed after 15 min irradiation in the presence of POR(H₂) and POR(In). No Survival was detected after 10 min of irradiation when **POR(H₂)-CIS/ZnS QDs-Silica** and **POR(In)-CIS/ZnS QDs-Silica** were utilized. In **Figure 5.3** the graph shows a slight increase at around 7-9 min. However, there is no significant increase in the Log value between 7-9 min as capped by the error bars. What looks like an increase is a result of the graph function, hence we have error bars to demonstrate the variability of the data and uncertainty in the reported measurement.

No increase is noted when the data is studied with consideration of the error bars.

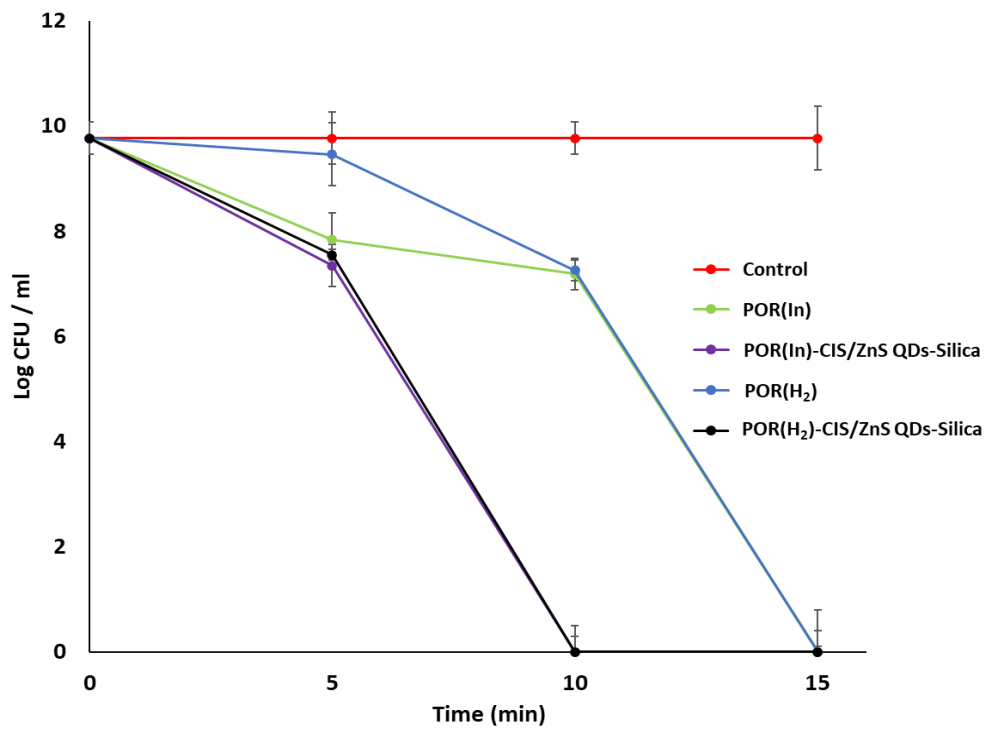


Figure 5.2. Logarithmic reduction of *S. aureus* under irradiation ($15.6 \mu\text{W}/\text{mm}^2$) with a concentration of $10 \mu\text{g}/\text{mL}$ of **POR(H₂)**, **POR(In)**, **POR(H₂)-CIS/ZnS QDs-Silica** and **POR(In)-CIS/ZnS QDs-Silica** using a Thorlabs 415 nm LED.

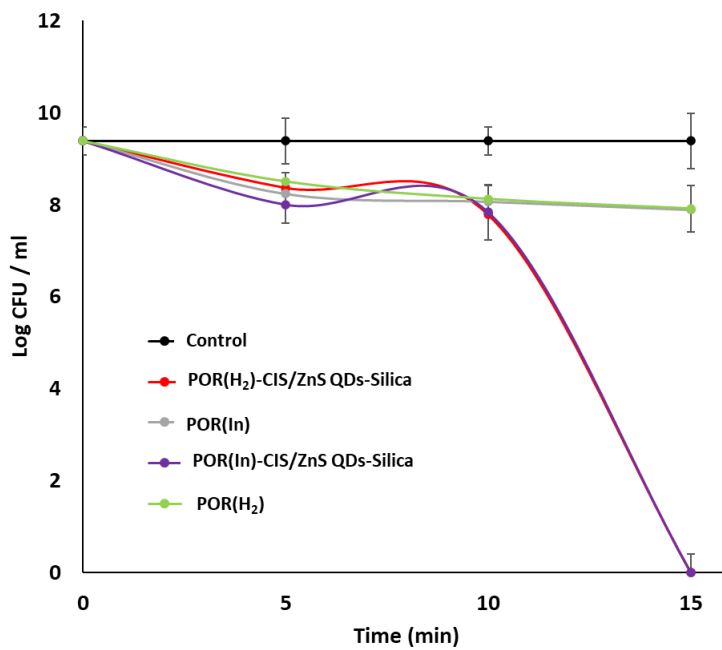


Figure 5.3. Logarithmic reduction of *E. coli* under irradiation (15.6 $\mu\text{W}/\text{mm}^2$) with a concentration of 10 $\mu\text{g}/\text{mL}$ of **POR(H₂)**, **POR(In)**, **POR(H₂)-CIS/ZnS QDs-Silica** and **POR(In)-CIS/ZnS QDs-Silica** using a Thorlabs 415 nm LED.

Table 5.6. Log reduction values for photoinactivation effect of **POR(H₂)**, **POR(In)**, **POR(H₂)-CIS/ZnS QDs-Silica**, **POR(In)-CIS/ZnS QDs-Silica** on *S. aureus* and *E. coli* in 15 min irradiation with Thorlabs M415L3 LED.

	Log reduction	
	<i>E. coli</i>	<i>S. aureus</i>
POR(H₂)	1.47	6.06
POR(In)	1.49	7.70
POR(H₂)-CIS/ZnS QDs-Silica	8.08	9.05
POR(In)-CIS/ZnS QDs-Silica	9.38	9.76

Table 5.7. % Bacterial viability of **POR(H₂)**, **POR(In)**, **POR(H₂)-CIS/ZnS QDs-Silica**, **POR(In)-CIS/ZnS QDs-Silica** for inactivation effect on *S. aureus* and *E. coli* in 15 min irradiation with Thorlabs M415L3 LED.

Time (min)	% Bacterial Viability					
	<i>E. coli</i>			<i>S. aureus</i>		
	5	10	15	5	10	15
POR(H₂)	13.12	5.47	4.26	8.65	0.31	0
POR(In)	7.96	5.09	3.32	1.16	0.26	0
POR(H₂)-CIS/ZnS QDs-Silica	4.35	2.82	0	0.67	0	0
POR(In)-CIS/ZnS QDs-Silica	9.58	2.49	0	0.37	0	0

5.3 REFERENCES

Hamblin, M.R., 2016. *Curr. Opin. Microbiol.* 33, 67–73.

Magaela, N.B., Makola, L.C., Managa, M., Nyokong, T., 2022. *J. Porphyr. Phthalocyanines* 26, 392–402.

Openda, Y.I., Ngoy, B.P., Muya, J.T., Nyokong, T., 2021. *New J. Chem.* 45, 17320–17331.

Sobotta, L., Skupin-Mrugalska, P., Piskorz, J., Mielcarek, J., 2019. *Eur. J. Med. Chem.* 175, 72–106.

CHAPTER 6

CONCLUSIONS AND RECOMMENDATIONS

6.1 CONCLUSIONS

This study was aimed at synthesizing and functionalizing QDs to achieve significant bacterial photoinactivation through combining the desirable properties of the QDs. This proceeded by synthesizing silica immobilized CuInS₂/ZnS quantum dots conjugated to metal-free and In (III) 4-(15-(4-boronophenyl)-10,20-diphenylporphyrin-5-yl)benzoic acid. Phototreatment of *S. aureus* and *E. coli* with the synthesized nanoconjugates then followed. Finally, examination of the physiochemical properties and antibacterial activity of the conjugates was explored.

The following conclusions were drawn from the research methods:

- Nanoconjugates comprising of metal-free or In(III) 4-(15-(4-boronophenyl)-10,20-diphenylporphyrin-5-yl)benzoic acid, CIS/ZnS QDs and mesoporous silica were sequentially synthesized.
- Various spectroscopic techniques were used for characterization of the nanoconjugates: The molecular structures of In (III) 4-(15-(4-boronophenyl)-10,20-diphenylporphyrin-5-yl)benzoic acid and metal-free derivative were elucidated using ¹H-NMR according to observed peaks. Mass spectrometry analysis of POR(H₂) molecular ion showed a peak at m/z = 701.8 corresponding to [M-H] and POR(In) showed a molecular ion peak at m/z = 853.4 corresponding to [M+3H]⁺. FTIR was also utilized to confirm functional groups such as aromatic -C-H at 2850 to 2921 cm⁻¹, C-N at 1581 cm⁻¹ and a B-C peak at 1012 cm⁻¹. UV/Vis spectroscopy revealed the presence of a Soret band and Q bands from the molecules. Red shifting occurred as a result of metalation. The final nanoconjugates showed absorption patterns characteristic of porphyrins, QDs and silica combined.
- Φ_F and Φ_Δ quantum yields improved for porphyrins in the presence of CIS/ZnS QDs, which enhanced the aPDI performance. Other characterizations such as XRD identified a polycrystalline and single-phase character formation as per XRD patterns. The nanoconjugates showed excellent thermal stability compared to individual porphyrin samples when TGA were employed. 90% of POR(H₂)-CIS/ZnS QDs-Silica and POR(In)-CIS/ZnS QDs-Silica mass was retained at 800 °C, compared to 50%

mass loss of unconjugated POR(H₂) and POR(In) at the same temperature. N₂ sorption studies suggested that the nanoconjugates presented type IV isotherms by the International Union of Pure and Applied Chemistry (IUPAC) classification.

- The study is evidence of improved photoinactivation through enhancement of ISC as a result of heavy atom effects. As such, the photoinactivation efficacy against *S. aureus* and *E. coli* was greatly improved.

- Conjugation of non-ionic porphyrins to nanomaterials with desirable properties is proven effective against *E. coli*.

- Utilization of mesoporous silica as a support has no negative effect on the photoinactivation efficacy of the nanoconjugate. Thus, it can be graded as a satisfactory support material since complete photoinactivation is achieved.

- Findings of the study were driven by aPDI in the presence of a porphyrin and quantum dots. POR(In)-CIS/ZnS QDs-Silica was the best performing conjugate with a singlet quantum yield of 0.72 and a log reduction of 9.38 and 9.76 against *Escherichia coli* and *Staphylococcus aureus*, respectively.

6.2 RECOMMENDATIONS

Recommendation of aPDI for microbial photoinactivation in water has been analyzed with VOSviewer. Several published papers from various publishers (Springer, Elsevier, Hindawi, etc) relating to aPDI have successfully utilized radiance to inactivate microbes in most cases. Photosensitizers, nanoparticles, semiconductors and polymeric materials are common drivers for these applications. However, the bibliometric analysis showed a limited amount of recovery and reusability studies on immobilized photoinactivators. Most studies are focused on antimicrobial lab scale experiments and less industrial experiments. Thus, future research in this field can focus on work that can be adopted by industry. Already synthesized and immobilized bioactive nanoconjugates with significant photoinactivation rates are to be employed for experiments such as emerging DBPs testing, broader microbial pools, disinfection rates vs volume, effect of water flow rates on nanoconjugate and many more.

Further research can also be conducted on long-term effects of intelligent nanomaterials in water applications on human health and the environment.

Additionally, it is crucial to study the economic impacts of supplementing conventional treatment methods with innovative technologies. As a missing aspect of this study, recovery and reusability of the synthesized nanoconjugates can be further investigated by the involved institute.